Investigation into Variable Phase Shift Keying using Direct Sequence Spread Spectrum Techniques

by

Clive V Whaits

National Higher Diploma *Cape Technikon*

Submitted to the Department of Electrical Engineering

in partial fulfillment of the requirements for the degree of

Master of Science in Electrical Engineering

at the

UNIVERSITY OF CAPE TOWN

April 1997

Signature of Author ..... Signed by candidate

C.V. Whaits
Department of Electrical Engineering
25 April 1997

Certified by .....

Dr. Robin M. Braun
Director of the Digital Modulation Research Group
Thesis Supervisor

Accepted by .....

Prof. Barry J. Downing
Head of Department

Declaration

I declare that this dissertation is my own work and is being submitted in partial fulfillment of the requirements for the degree of Master of Science in Engineering at the University of Cape Town. It has not been submitted before for any degree at this or any other academic institution. All consulted literature completely listed in the references.

Signed by candidate

C. V. Whaits
Candidate

Acknowledgments

I wish to thank Dr. Robin M. Braun for his constructive support, guidance and astute supervision during this research project. Special thanks are due to my friends and colleagues of the Digital Communications Research Group at the University of Cape Town, especially Dr. Johan G. van de Groenendaal and Dirk Kohlen, for the many extremely useful discussions, friendly support and encouragement.

I would also like to express my sincere gratitude to my colleagues at the Cape Technikon, Department of Electrical Engineering, in particular Rob Neilson and Egon Voss, for their continuous words of support and encouragement during this demanding task.

I would also like to thank all my close friends for all their tremendous support and who took a special interest my work, especially Victor and Alicia Gibson.

I am deeply indebted to my dear wife Ronél and my children Shelley and Grant, for their patience, love and never ending support during a very trying period of my life.

Last but not least, I would like to thank my Lord and God, for the health, stamina and ability to tackle and complete this project.

Abstract

This thesis reports the research done into a relatively unknown modulation scheme called VPSK (Variable Phase Shift Keying) and the use of DSSS (Direct Sequence Spread Spectrum) techniques to achieve carrier synchronization and hence coherent demodulation in the receiver.

VPSK is a new and relatively unknown modulation scheme in which data bits are encoded using patented algorithms designed by Miller and Walker. VPSK modulation is a SSBSC (Single Sideband Suppressed Carrier) modulation scheme with good bandwidth efficiency. Data is coherently demodulated in the receiver. In existing VPSK systems, the locally generated carrier in the receiver is synchronized to an integer multiple of the symbol clock frequency to allow coherent demodulation. This coherent method of demodulation is not optimum if the channel over which information must be transmitted is a non-Gaussian channel, or has multi-path characteristics.

It is the aim of this thesis to investigate an alternative method of synchronisation to achieve coherent demodulation of a VPSK modulated signal. The technique used in this thesis is DSSS, where the PN (pseudo random noise) chipping frequency used to spread the VPSK signal in the transmitter, is, after being recovered in the receiver, used to derive the locally generated carrier and symbol clock signals. This alternative method of carrier synchronization using DSSS techniques, which has well known performance enhancements in multi-path interference rejection, is applied to the relatively unknown VPSK digital modulation scheme in an effort to improve coherent detection with the additional possibility of increased performance.

Preface

Variable phase shift keying (VPSK) is a relatively new digital modulation scheme which uses slip encoded data signals and single side band suppressed carrier modulation techniques. Single side band suppressed carrier modulation is commonly used in analog communication systems, but seldom used in digital modulation schemes.

One of the more difficult aspects of single side band suppressed carrier demodulation, is the synchronisation of the locally generated carrier and symbol clock signals. The main purpose of this dissertation concerns the designing of a functional variable phase shift keying digital communications system, which uses direct sequence spread spectrum techniques to enable synchronous demodulation in the receiver. Although the design uses line encoded data and spread spectrum techniques, this dissertation is not concerned with the study of coding or processing gain.

The dissertation concentrates on the design of a functional 2-VPSK System, using the SystemView computer simulation software package to simulate the operation of this 2-VPSK System.

Contents

List of Figures

List of Tables

Chapter 1

Introduction

1.1 Variable Phase Shift Keying Modulation

Variable Phase Shift Keying (VPSK) modulation is Binary Phase Shift Keying (BPSK) in which one's and zero's are represented by 180° phase changes of the carrier. VPSK modulation is a relatively new and somewhat unknown digital modulation scheme with good bandwidth efficiency.

VPSK is a digital modulation method that compresses the RF data transmission bandwidth. 2-VPSK has 4 bits per Hertz and 10-VPSK 15.3 bits per Hertz [2]. When compared to other traditional methods of modulation such as QAM, VPSK does not suffer a degradation in signal to noise ratio when the number of bits per Hertz is increased [3]. In other words, VPSK is closer to the Hartley-Shannon limit.

VPSK does not use multiple bits such as dibits or tribits, as does an I/Q (inphase/quadrature) system like QAM, to increase the bandwidth efficiency. The enhanced bandwidth efficiency (compression) obtained in VPSK is due to the spectral characteristics of the slip coded data. The VPSK spectrum is known as a Digital Biphase Spectrum [2] and as opposed to a NRZ (Non-return to Zero) line coded spectrum, and it has a minor d.c. component. The VPSK spectrum extends from approximately $0.25R_b$ to $0.5R_b$ as shown in Chapter 2, Figure 2.2.

2-VPSK differs from ordinary BPSK in that the bit widths of the data information, prior to

modulation, are varied according to an algorithm patented by Miller [1] in 1963. This information data format is a class of Slip Code and is often referred to as Miller Code, MFM (Modified Frequency Modulation) or Delay Modulation.

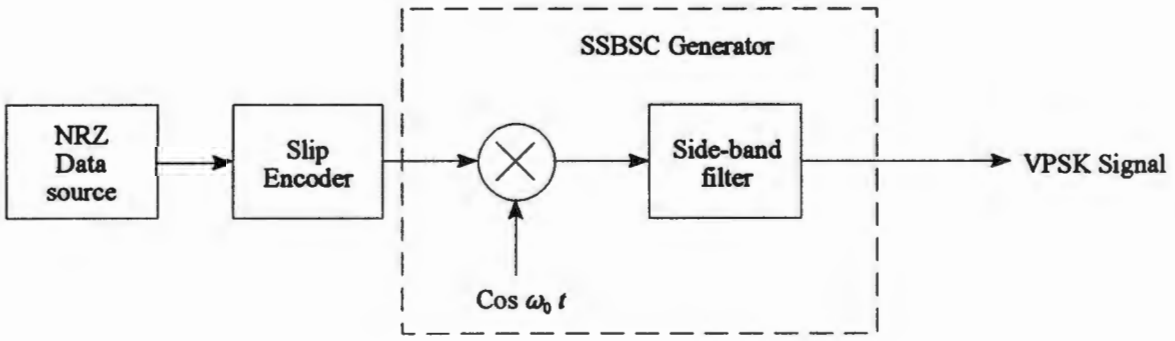

Figure 1.1: VPSK Digital Modulation Scheme.

The VPSK modulation scheme comprises a two step process as shown in Figure 1.1. The first step involves encoding the data using what is known as a Slip Coding technique. A Slip Code is a coding method that stretches the pulse width of the incoming data. This new slip coded data is then modulated onto a carrier using the well known SSBSC modulation technique. This two step process is what is referred to in the literature as VPSK modulation.

If the incoming data bit widths are varied (slipped) by 2/2, 3/2 or 4/2 times the original bit width, then we have what is known as a 2,3,4 Slip Code [2]. When this 2,3,4 Slip Code is modulated on to a carrier using SSBSC techniques, we have what is known as 2-VPSK. Higher Slip Codes exist, where the transmitted bit widths are stretched by fractions of the original bit width, depending on the order of the VPSK modulation scheme.

For example, a 6-VPSK modulation scheme has 6 clock periods per bit period and the coded pulse train has periods of 6/6, 7/6 and 8/6 times the original bit period, depending on the incoming data. The higher order VPSK patents are owned by H.R. Walker [4][5].

1.2 Spread Spectrum Modulation and Demodulation

1.2.1 A Brief History

Spread spectrum had its origin in the United States Military [6] where communications between friendly communicators was susceptible to detection and interception by the enemy, or vulnerable to intentionally introduced unfriendly interference called jamming. Communication systems that employed spread spectrum to reduce the communicator's detectability and combat jamming are referred to as LPI (low probability of intercept) and AJ (anti-jam) communication systems.[6]

The subsequent change in the world political situation reduced the emphasis on using spread spectrum techniques for their original purposes and a host of new commercial applications for spread spectrum has evolved, particularly in the area of cellular mobile communications. Other applications of spread spectrum communications include [7]:

- Selective addressing.
- Low-density power spectra for signal hiding.
- Message screening.
- High resolution ranging.
- Intentional interference rejection.
- Multipath interference rejection.

1.2.2 What is Spread Spectrum?

Spread spectrum is a communication technique wherein the transmitted modulation is spread (increased) in bandwidth prior to transmission over the channel and then despread (decreased) in bandwidth by the same amount at the receiver. If it were not for the fact that the communication channel introduces some form of narrowband (relative to the spread

bandwidth) interference, the receiver performance would be transparent to the spreading and despreading operations (assuming that they are identical inverses of each other). That is, after despreading the received signal would be identical to the transmitted signal prior to spreading [6].

In the presence of narrowband interference, however, there is a significant advantage to employing the spreading/despreading procedure described. The reason for this is as follows. Since the interference is introduced after the transmitted signal is spread, then, whereas the despreading operation at the receiver shrinks the desired signal back to its original bandwidth, at the same time it spreads the undesired signal (interference) in bandwidth by the same amount, thus reducing its power spectral density. This, in turn, serves to diminish the effect of the interference on the receiver performance, which depends on the amount of interference power in the spread bandwidth. This very simple explanation is at the heart of all spread spectrum techniques [6].

To be classified as a spread spectrum system, the system must have the following characteristics:

- The transmitted signal energy must occupy a bandwidth which is larger than the information bit rate (usually much larger) and which is independent of the information bit rate.
- Demodulation must be accomplished, in part, by correlation of the received signal with a replica of the signal used in the transmitter to spread the information signal.

A number of other modulation schemes, for example low-rate coding and wide band FM [8], also use wider bandwidths but are not classified as spread spectrum systems. Spread spectrum systems can be classified into three primary groups, namely

- Direct Sequence Spread Spectrum.
- Frequency-hopped Spread Spectrum.
- Time-hopped Spread Spectrum.

Each of these methods have their respective advantages and disadvantages [7]. In this dissertation, only DSSS is considered, and therefore any reference to a spread spectrum system will imply DSSS unless otherwise stated.

1.2.3 Direct Sequence Spread Spectrum Modulation

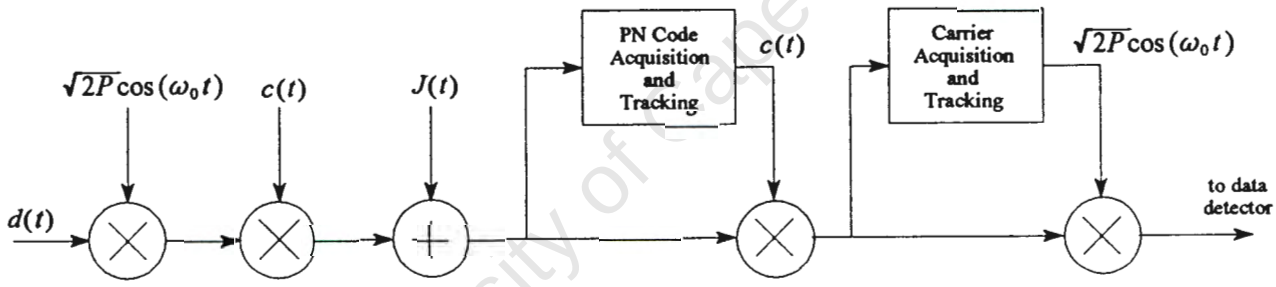

Figure 1.2: A DSSS Modulation System

DSSS is a very common form of spread spectrum whereby the spectrum of a data modulated carrier, typically that of a BPSK signal, is spread using a very wideband spreading signal or code. That is, a BPSK signal is modulated a second time with this wideband spreading signal and indicated as $c(t)$ in Figure 1.2. The spreading signal, PN code, or chipping signal is chosen to have properties which facilitate demodulation of the transmitted signal in the intended receiver, and which make demodulation by an unintended receiver as difficult as possible.

These same properties will also make it possible for the intended receiver to discriminate between the wanted signal and any intentional interference signal. If the bandwidth of the

spreading signal is large relative to the data bandwidth, the spread spectrum transmission bandwidth is dominated by the spreading signal and is virtually independent of the data signal [8]. In practical systems, the bandwidth of the transmitted signal is limited to twice the chipping rate. The carrier frequency should be chosen so that no spectral fold-over occurs, and the chipping frequency chosen such that no self interference takes place [9].

In the receiver, the local PN sequence generator is synchronised to within one chip of the PN waveform of the received signal by the PN code acquisition and tracking loop. This local PN chipping signal is ideally an exact replica of the PN sequence in the transmitter, and is then used to despread the received signal, resulting in the original BPSK signal. The local carrier frequency is then synchronised with that in the transmitter in the carrier synchronisation and tracking loop, so that coherent demodulation of the BPSK signal can be achieved, resulting in the original data being recovered.

1.3 Shortcomings in the Demodulation of VPSK

In a VPSK system, the translation of the SSBSC signal back to baseband is achieved by means of coherent demodulation. In a digital SSBSC system like VPSK, the original carrier and one of the sidebands is removed, thus the locally generated carrier must be exactly coherent with the original carrier in the transmitter for proper demodulation to be achieved.

The patent holder of the VPSK modulation schemes, H.R. Walker, uses an integer multiple of the symbol clock frequency to synchronise the locally generated carrier with that in the transmitter [8]. This method of carrier synchronisation works reasonably well as long as the received carrier is close enough to the transmitted carrier to allow carrier acquisition and tracking to occur, and hence synchronous demodulation to take place. This VPSK system has been theoretically validated in terms of functionality and the Hartley-Shannon channel capacity theorem [10]. However, this method of carrier synchronisation may fail if the channel is non-

linear, the transmitted signal is affected by doppler shift or the channel has multipath characteristics. Figure 1.3 shows the block diagram of an original VPSK system as used by Walker.

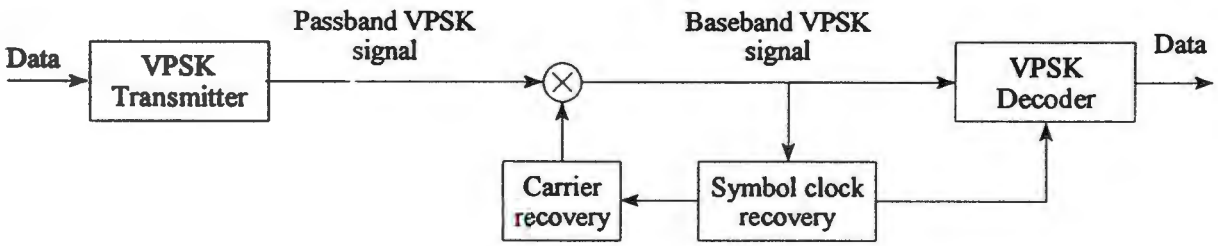

Figure 1.3: Block diagram of original VPSK system.

In this thesis, the design and implementation of a simulated 2-VPSK communications system, which utilises the properties of a DSSS signal for carrier and symbol clock recovery, is described. The aim of the thesis is to research another method of achieving coherent demodulation of a VPSK signal.

1.4 How DSSS can be used for Coherent Demodulation of VPSK

If the original carrier and the PN chipping signal in the transmitter are made functions of the symbol clock frequency, then, when the PN signal is recovered in the receiver, it can be used to derive the locally-generated carrier and symbol clock signals.

A block diagram of the proposed direct sequence spread spectrum variable phase shift keying modulation system is shown in figure 1.4.

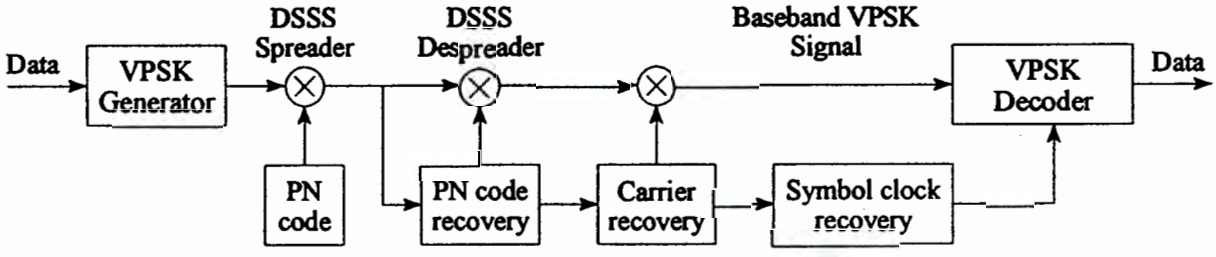

Figure 1.4: Block diagram of proposed DSSS VPSK system.

Chapter 2

Encoding Base Band Data into Miller Code

In Chapter 1 the basic principles of VPSK modulation were introduced. The generation of a VPSK signal involves a two step process. The first step entails the encoding of the raw incoming NRZ data into a slip code and then modulating this slip coded data onto a sinusoidal carrier using a SSBSC modulator. This class of modulation uses a line code class where pulse width changes are used to compress the bandwidth of the transmitted signal. In this chapter a detailed description of the process of Miller Line coding is presented.

2.1 Deriving a Slip Coded Line Code

Slip coded signals fall into one of the major classes of binary line codes called transition codes. Transition codes carry information in the change in level appearing in the line coded waveform [6]. Transition codes generally have memory, using past binary data to dictate present form. The encoded line code is obtained from the incoming bipolar NRZ data by using a technique called slip coding. A slip code is derived from a coding method that changes the pulse width of the incoming data [3]. That is, slip coding is a form of pulse width modulation where the width of a pulse is stretched by a fraction of the pulse period.

In the encoding procedure, each input data bit has a period of M clock periods and the data bit polarity changes are phase shift key coded with waveform widths of M/M, $M + 1/M$ and

$M+2/M$ bit periods wherein M is an integer equal to 2 or greater [5]. Any value of M of 2 or greater can be used, but the circuitry is greatly simplified if even values are used [5]. Each of the incoming data bits is encoded into a digital signal which toggles between 1 and -1 polarities, and has time periods greater than multiples of the clock period. The width of the encoded pulse depends on whether or not the polarity of the data bit is changed from that of the previous data bit.

As an example, consider the generation of a slip coded signal for a 6-VPSK modulation scheme. The slip coded signal is obtained according to the following rules [5]:

1. When the present data bit is the same as the previous one, that is no polarity change, the encoded signal is switched to the opposite polarity with a pulse width of (M/M) bit periods after the previous change in polarity. In this example, $M = 6$.

2. When the present data bit polarity is changed from that of the previous data bit, (changes from 1 to 0 or vice versa), the polarity of the encoded signal is switched with a pulse width of $M+1/M$ bit periods (here 7/6) after the previous change.

3 Upon encountering the $(M-1)^{th}$ data bit polarity change, (in this case the 5^{th}) the encoded signal is given a width of $M+2/M$ bit periods after the previous polarity change. This $M+2/M$ pulse width (8/6 in this case) is only transmitted when the input data train is a 1 0 1 sequence.

Due to the encoded data train having bit periods which are wider than the original data bit periods, after $(M-1)$ counted data bit polarity changes, the last data bit in each encoding cycle is to be omitted. At the receiving end, the encoded signal is decoded by a complimentary algorithm which also restores the omitted bit.

A number of VPSK modulation schemes, each with a different slip code, have been invented [4][5], and are shown in Table 2.1. These patented VPSK modulation schemes are categorised by the different slip coding algorithms used for data encoding. For example, in the 8-VPSK modulation scheme the modulation level is $M = 8$, and each input data bit has a period equal to 8 clock periods. The encoded waveform is a 8,9,10 slip code, which means that the encoded bit widths will be 8/8,9/8 and 10/8 times the input data bit widths.

Scheme	*Data Encoding Method*	*Slip*
1-VPSK	Manchester	1,2
2-VPSK	Miller	2,3,4
4-VPSK	Walker	4,5,6
6-VPSK	Walker	6,7,8
8-VPSK	Walker	8,9,10
10-VPSK	Walker	10,11,12

Table 2.1: VPSK modulation schemes with the respective slip codes [3].

2.2 The Miller Line Code

The Miller line code is a 2,3,4 slip code which is also known as MFM (Modified Frequency Modulation) or Delay Modulation [4][11]. It is an encoding technique which converts binary NRZ data into a digital signal having time periods greater than multiples of the clock period.

The frequency spectrum of the Miller encoded signal is a biphase spectrum with minor d.c. component [6]. Its power is concentrated into a very narrow band which lies just below half the bit rate. This Miller encoding technique is widely used in magnetic disk recording to narrow the bandwidth required by the recording head and storage media [4][12]. The Miller encoding system uses a simplified slip coding algorithm to the one presented in para 2.1 above,

presented in para 2.1 above, and which consists of the following rules [11]:

1. A transition from one level to the other is placed at the midpoint of the bit period when the input binary data contains a "one".

2. No transition is used if the input binary data contains a "zero" unless it is followed by another "zero", in which case the transition is placed at the end of the bit period of the first "zero".

The operation of the Miller encoding algorithm on a NRZ input signal is illustrated in Figure 2.1. In this example the relationship between the clock signal, the NRZ data signal and the resulting slip coded Miller signal is clearly illustrated.

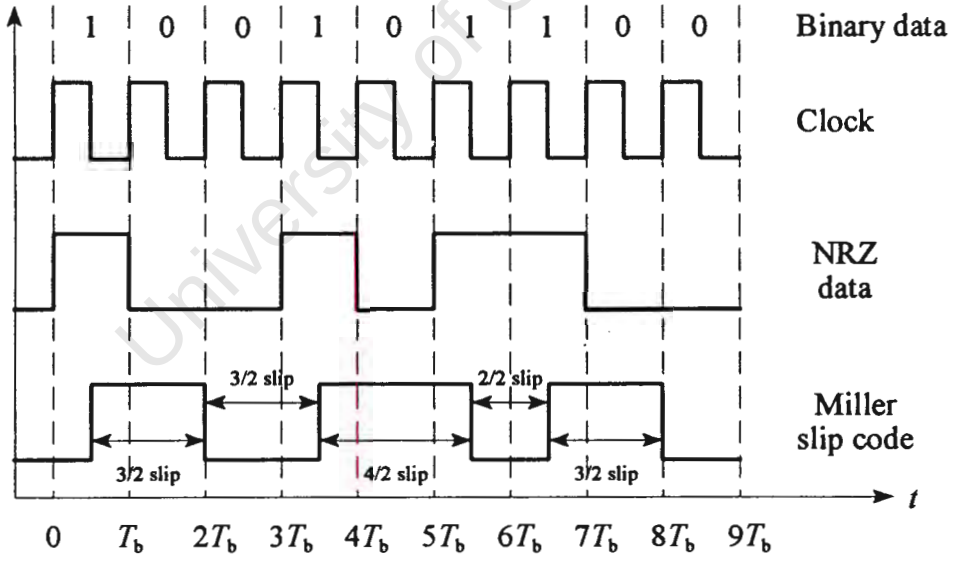

Figure 2.1: Waveforms of the clock, NRZ and Miller encoded signals.

As is clearly evident from Figure 2.1, the format utilised by the Miller encoding system employs bit widths of 1, 1.5 and 2 times the original input NRZ data bit width. This means

that the time periods of the encoded signal are 2,3 and 4 times the clock period. It can also be clearly seen that the Miller encoding system produces signals that are at ¼ of the clock rate for a 101 input bit pattern, at ⅓ of the clock rate for 100 or 001 input bit patterns and at ½ of the clock rate for 00 and 11 bit patterns.

In this dissertation, a 2-VPSK system is simulated, which uses the above procedure for generating the Miller line coded data signal in this 2-VPSK system.

2.3 Spectral Properties of Slip Coded Signals

In order to compare the spectral properties of slip coded signals, the power spectral density of three line codes is presented in figure 2.2

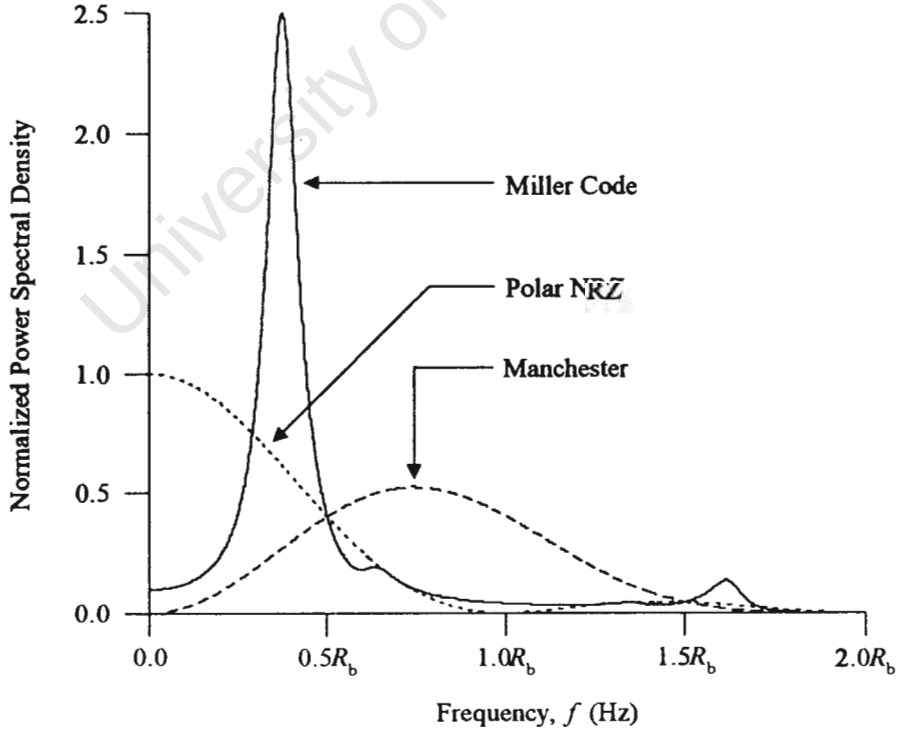

Figure 2.2: Power spectral density of different line codes, where $R_b = 1/T_b$ is the bit rate.

The spectrum of a NRZ with equally likely bits is given by [6]:

$$S(f) = V^2 T \left(\frac{\sin \pi f T}{\pi f T} \right)^2 \tag{2.1}$$

The power spectral density of this NRZ line code signal centres about 0 Hz and contains a large d.c. component. The first null for this NRZ signal is at R_b Hz. The power spectral density of the Miller slip code for equally likely data is given by [6]:

$$\begin{aligned} S(f) = & \left[\frac{V^2 T_b}{2[\pi f T_b]^2 [17 + 8\cos(8\pi f T_b)]} \right] \\ & \times [23 - 2\cos(\pi f T_b) - 22\cos(2\pi f T_b) \\ & - 12\cos(3\pi f T_b) + 5\cos(4\pi f T_b) + 12\cos(5\pi f T_b) \\ & + 2\cos(6\pi f T_b) - 8\cos(7\pi f T_b) + 2\cos(8\pi f T_b)] \end{aligned} \tag{2.2}$$

This spectrum clusters from about $0.25R_b$ Hz to just below $0.5R_b$ Hz and has a very small d.c. content. As the order of the slip encoding is increased the power spectrum becomes narrower with increasing order of slip. This means that as the order of M is increased, the power spectral density of each M-VPSK modulation scheme clusters in an increasingly smaller spectral area just below $0.5R_b$ Hz [8].

Table 2.2 [8] is an extension of Table 2.1 and is presented to show the various orders of VPSK modulation schemes, the data encoding method, the order of slip coding used, the power spectral density spread and the bandwidth efficiency of each scheme.

Scheme	*Data encoding method*	*Slip*	*Spread*	*Bits / Hz*
1-VPSK	Manchester	1,2	$0.5R_b$ to $1.0R_b$	2
2-VPSK	Miller	1,2,3	$0.25R_b$ to $0.5R_b$	4
4-VPSK	Walker	4,5,6	$0.36R_b$ to $0.5R_b$	7.4
6-VPSK	Walker	6,7,8	$0.4R_b$ to $0.5R_b$	10
8-VPSK	Walker	8,9,10	$0.42R_b$ to $0.5R_b$	12.6
10-VPSK	Walker	10,11,12	$0.435R_b$ to $0.5R_b$	15.3

Table 2.2: Comparison of various VPSK modulation schemes.

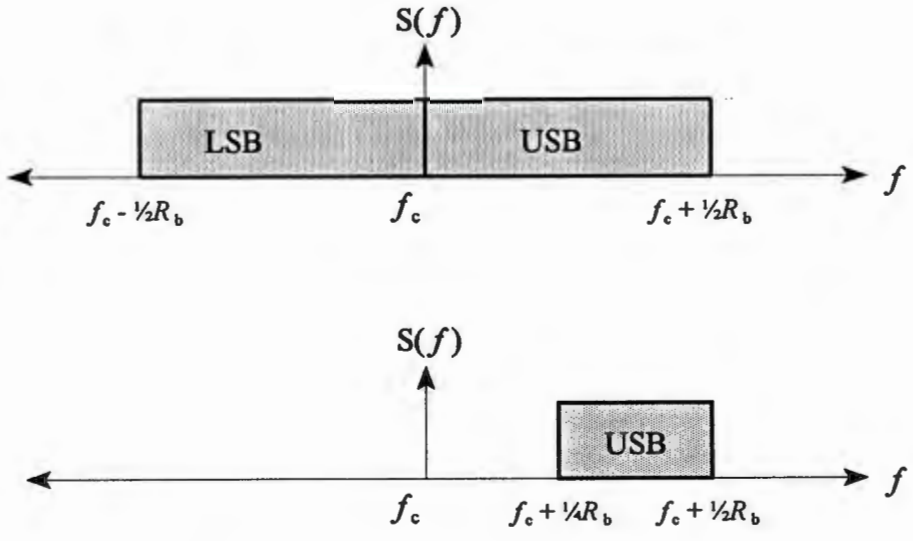

Figure 2.3: The Passband Power spectrums of a BPSK and a 2-VPSK modulation scheme.

When only the USB (upper sideband) is transmitted, as is the case with VPSK modulation schemes, then varying degrees of bandwidth efficiency are obtained.

For example, consider the 2-VPSK scheme. The bandwidth efficiency is given by

$$\eta_{BW} = \frac{R_b(\text{bps})}{BW(\text{Hz})} \tag{2.3}$$

The energy of a Miller slip code scheme lies between $0.25R_b$ and $0.5R_b$. Now when this Miller encoded data is modulated on to a carrier using SSBSC techniques, and only the USB is transmitted as shown in Figure 2.3, then the transmitted bandwidth is

$$BW = 0.5R_b - 0.25R_b = 0.25R_b$$

Thus

$$\eta_{BW} = \frac{R_b}{0.25R_b} = 4 \text{ bps/Hz}$$

In the higher order VPSK modulation schemes, even better bandwidth efficiency is achieved [2][3][8].

2.4 The Power Spectrum of a Miller Line Code

To analyse the Miller waveform it is necessary to divide each bit interval into two half intervals, then each bit interval can be described by the levels occurring in the two half bit intervals. Choosing the two possible levels as -1 and +1, the four types of bit intervals or states that can occur are (+1, +1); (+1, -1); (-1, +1) and (-1,-1). For the Miller code, the four elementary signals which represent a binary 1 and 0 respectively are defined by

$$s_1(t) = -s_4(t) = A \qquad \text{for } 0 \le t \le T_b \tag{2.4}$$

and

$$s_2(t) = -s_3(t) = \begin{cases} +A & \text{for } 0 \le t < \frac{T_b}{2} \\ -A & \text{for } \frac{T_b}{2} \le t \le T_b \end{cases} \tag{2.5}$$

where T_b is the bit period.

Since each bit depends only on the previous state and the given binary data, the sequence of states that is generated is a first-order Markov process with four states [13]. The Markov process is completely described by those four states and a set of a priori (stationary) and transition probabilities. It is assumed that the binary data consists of random independent bits, hence the stationary probabilities for Miller code are equiprobable and equal to ¼.

The probability of transition, $p_{ik} = p(k|i)$, is the conditional probability that the signal $s_k(t)$ is transmitted in any given interval after the occurrence of the signal $s_i(t)$ in the previous transmission interval. The transition probabilities for a Miller line code, modelled as a Markov source, are arranged in a probability of transition matrix $[P_{ik}]$, and defined by

$$[P_{ik}] = \begin{bmatrix} 0 & ½ & 0 & ½ \\ 0 & 0 & ½ & ½ \\ ½ & ½ & 0 & 0 \\ ½ & 0 & ½ & 0 \end{bmatrix} \tag{2.6}$$

The matrix element values are determined as follows, given that the columns represent the transition probabilities for $s_1(t)$, $s_2(t)$, $s_3(t)$ and $s_4(t)$ respectively.

1st row: If the previous bit interval is $s_1(t)$, that is a $[+1,+1]$, due to the encoding algorithm it is impossible for the transmission interval to be either a $s_1(t)$ or $s_3(t)$. Thus the associated transmission probabilities are 0. Since the two remaining states are equally likely, the associated transmission probabilities are both equal to ½.

2nd row: If the previous bit interval is $s_2(t)$, that is a [+1,-1], it is impossible for the transmission interval to be either a $s_1(t)$ or $s_2(t)$. Thus the associated transmission probabilities are 0. The two remaining states are equally likely and the associated transmission probabilities are both equal to ½.

3rd row: If the previous bit interval is $s_3(t)$, that is a [-1,+1], it is impossible for the transmission interval to be either a $s_3(t)$ or $s_4(t)$. Thus the associated transmission probabilities are 0 and the two remaining states are equally likely, hence the associated transmission probabilities are both equal to ½.

4th row: If the previous bit interval is $s_4(t)$, that is a [-1,-1], it is impossible for the transmission interval to be either a $s_2(t)$ or $s_4(t)$. Thus the associated transmission probabilities are 0 and the two remaining equally likely states have transmission probabilities both equal to ½.

Another property of the Miller line code is that it satisfies the recursion relation

$$[P]^{4+l}[S] = -\tfrac{1}{4}[P]^{l}[S] \qquad l \geq 0 \tag{2.7}$$

where $[S]$ is the signal correlation matrix whose ik^{th} element is defined by

$$s_{ik} = \frac{1}{T_b}\int_0^{T_b} s_i(t)\, s_k(t)\, dt \qquad i, k = 1, 2, 3, 4 \tag{2.8}$$

From this statistical description of the Miller line code, the power spectral density of a data sequence generated by this source is given by [14]:

$$S(f) = \frac{1}{T_b^2} \sum_{n=-\infty}^{\infty} \left| \sum_{i=1}^{N} p_i S_i\left(\frac{n}{T_b}\right) \right|^2 \delta\left(f - \frac{n}{T_b}\right)$$

$$+\frac{1}{T_b} \sum_{i=1}^{N} p_i |S_i(f)|^2$$

$$+\frac{2}{T_b} \Re\left\{ \sum_{i=1}^{N} \sum_{k=1}^{N} p_i S_i^*(f) S_k(f) p_{ik}\left[e^{-j2\pi f T_b}\right] \right\} \qquad (2.9)$$

where:

$\delta(f)$ is the Dirac delta function,

$S_i(f) = \int_0^{T_b} s_i(t) e^{-j2\pi f t}\, dt$ is the Fourier transform of the i^{th} elementary signal, and

$$p_{ik}(z) = \sum_{n=1}^{\infty} p_{ik}^{(n)} z^n \qquad (2.10)$$

In equation (2.9), the asterisk denotes complex conjugate. The quantity $p_{ik}^{(n)}$ is defined as the probability that the elementary signal $s_k(t)$ is transmitted n signalling intervals after the occurrence of $s_i(t)$. Hence from the properties of Markov sequences, $p_{ik}^{(n)}$ is the ik^{th} element of the matrix $[P]^n$. Also by definition, $p_{ik}^{1} = p_{ik}$.

Many special classes of signals exist for which the general power spectral density result of equation (2.9) can be simplified. The first simplification is the line spectrum of equation (2.9), which disappears when [15]:

$$\sum_{i=1}^{N} p_i S_i\left(\frac{n}{T_b}\right) = 0 \qquad (2.11)$$

which implies that a necessary and sufficient condition for the absence of a line spectrum is that

$$\sum_{i=1}^{N} p_i s_i(t) = 0 \tag{2.12}$$

Thus the Miller line code is described by the four signal states $s_i(t)$ where $i = 1, 2, 3$ and 4 and where each binary number is represented by a set of antipodal signals which follow the relation $s_i(t) = -s_j(t)$ where $i, j \in [1,2,3,4]$. Since the a priori stationary probabilities of a Miller line code are all equal, equation (2.12) applies to a Miller line code and results in a continuous spectrum free of any Dirac delta components.

Substituting equations (2.4) and (2.5) into equation (2.8) and arranging the results in the form of a matrix, yields

$$[S] = \begin{bmatrix} 1 & 0 & 0 & -1 \\ 0 & 1 & -1 & 0 \\ 0 & -1 & 1 & 0 \\ -1 & 0 & 0 & 1 \end{bmatrix} \tag{2.13}$$

Finally, using equations (2.6), (2.7) and (2.13) in the general power spectral density result of equation (2.9) yields the following result for the Miller line code for equally likely data [15]:

$$\begin{aligned} \frac{S(f)}{E_b} = & \left[\frac{1}{2\theta^2[17 + 8\cos(8\theta)]}\right] \\ & \times [23 - 2\cos\theta - 22\cos(2\theta) \\ & - 12\cos(3\theta) + 5\cos(4\theta) + 12\cos(5\theta) \\ & + 2\cos(6\theta) - 8\cos(7\theta) + 2\cos(8\theta)] \end{aligned} \tag{2.14}$$

where $\theta = \pi f T_b$ and $E_b = A^2 T_b$.

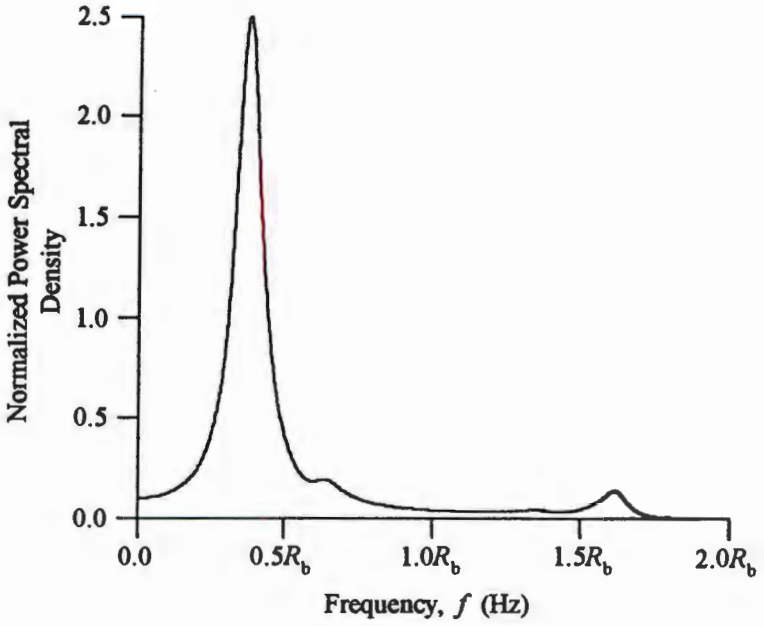

Figure 2.4: Power spectral density of a Miller line code derived from equation 2.14.

When looking at equation (2.14), it is clearly evident that the second harmonic contributes significantly to the power spectrum of the Miller code. Figure 2.4 indicates that most of the energy in a Miller code is contained in less than $0.5R_b$ Hz. The diagram in figure 2.4 shows that the Miller code has a minor d.c. component [6].

2.5 The Simulated Miller Line Code

In this section, a detailed description of the method used to simulate the Miller line code is presented.

2.5.1 Generation of the Miller Line Code

As indicated in Figure 2.5, the Miller encoding process consists of three processes:

(a) Generation of the bit stream using a pseudo random source.

(b) Mapping the random bit stream into Miller code.

(c) Conversion of the Miller code into a bipolar data stream.

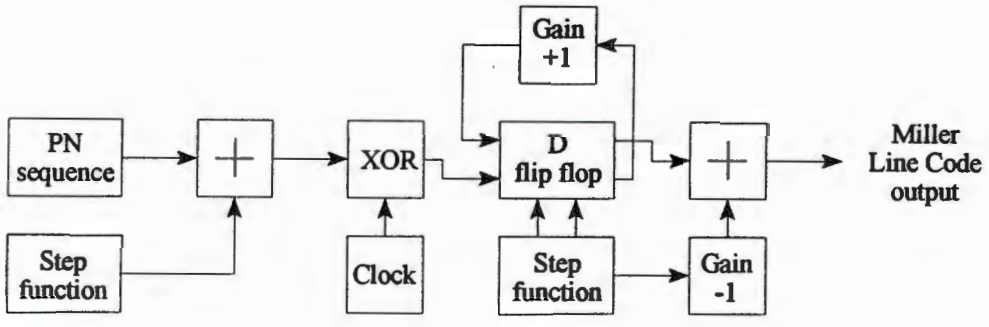

Figure 2.5: Block Diagram of Miller Line Encoder.

In the SystemView simulator used in this thesis, block functions are easily implemented using the available library of system tokens. The random bit stream generation is realised by using the PN sequence generator token and summing its output with a d.c. voltage source, implemented by using a step function starting at $t = 0$, to provide a unipolar NRZ random data stream.

Next, the random data stream is mapped into a Miller code. First the unipolar NRZ signal is converted into a unipolar Biphase code and then every second transition is deleted. These steps are implemented by XOR-ing the NRZ data stream with a system clock signal, and then applying the output to a D-Flip-flop which provides a unipolar Miller encoded signal. Finally, the bipolar Miller code is obtained by adding the unipolar Miller data stream to a suitable d.c. voltage obtained from a step function as shown in Figure 2.5.

An example of the Miller slip encoded signal and the resulting power spectrum are shown in Figure 2.6 and 2.7 respectfully.

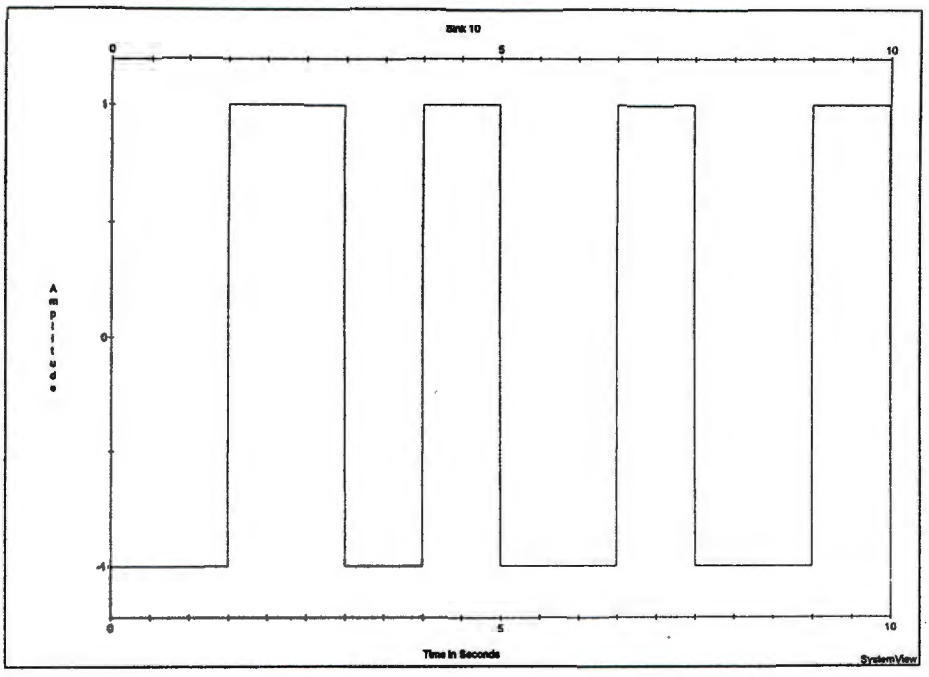

Figure 2.6: Miller line code generated in the simulation.

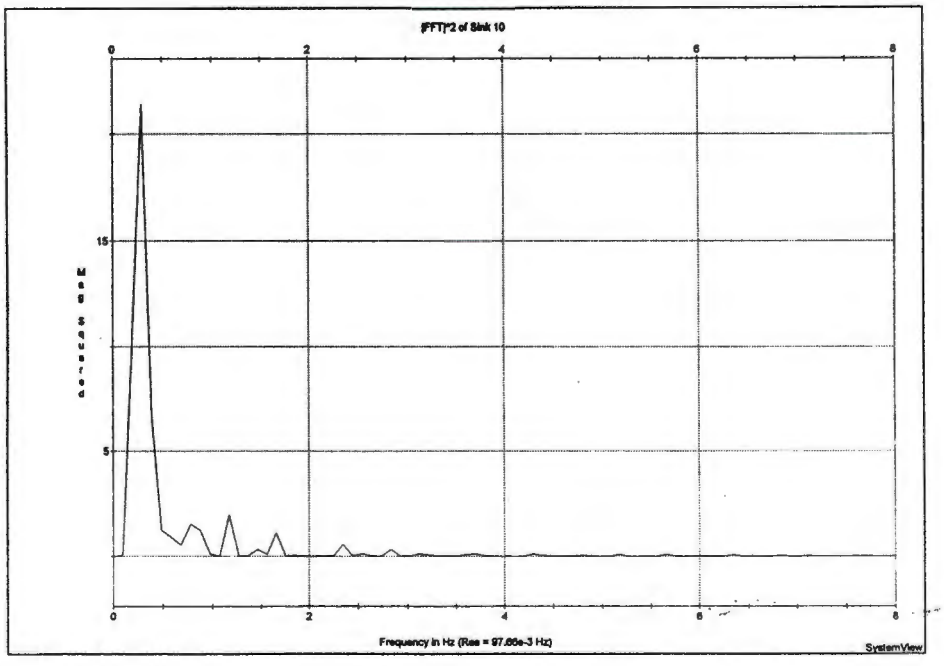

Figure 2.7: Power spectrum of the simulated Miller line code.

Chapter 3

Generation of the VPSK Signal

In Chapter 2, the first step in the process of the generation of a VPSK modulation signal was presented. This involved the encoding of the NRZ data signal into a Miller line code according to a patented algorithm. In this chapter the final stage in the generation of a VPSK modulation signal is presented, that is the SSBSC method of modulation.

Modulation methods that transmit only the upper or lower sideband of a DSBSC (double sideband suppressed carrier) signal are called SSBSC (single sideband suppressed carrier) signals. In SSBSC modulation, either the USB (upper sideband) or LSB (lower sideband) of the original DSBSC signal may be transmitted. The USB and LSB have even amplitude and odd phase symmetry about the carrier frequency [16], thus either sideband contains sufficient information to recover the information signal.

When compared to DSBSC modulation, which requires a bandwidth of twice the highest original information signal, SSBSC modulation only requires the bandwidth of the original information signal. Thus SSBSC signals are more bandwidth efficient than DSBSC signals as they require only half as much bandwidth.

If the information signal is a Miller line encoded signal, as is the case in a VPSK modulation scheme, the transmitted bandwidth is even narrower than in conventional SSBSC systems as the modulated spectrum is spread between $f_c \pm \frac{1}{4}R_b$ and $f_c \pm \frac{1}{2}R_b$ as shown in figure 2.4 for

the USB case. However, the increased bandwidth efficiency of a VPSK modulation scheme is somewhat offset by the increased system complexity and susceptibility to frequency and phase errors in the demodulation process [17].

3.1 Generation of SSBSC Signals

Two methods are commonly used to generate SSBSC signals. The first and conceptually simple method is the filter method, in which a DSBSC signal is generated and then the unwanted sideband is filtered out using a bandpass filter. The filter method requires very sharp roll-off characteristics for the bandpass filter to prevent adjacent channel interference.

The second method is known as the phase shift method where 90° phase shift networks are used to generate a SSBSC signal. Again, stringent requirements are necessary for the phase shift networks to ensure that all frequency components of the information signal are shifted by 90°. These phase shift networks are generally a Hilbert transformer and are practically implemented with a linear phase FIR (finite impulse response) filter. Better suppression of the unwanted sideband is achieved using the phase shift method of SSBSC generation, but this approach requires the use of complicated digital FIR filters.

The stringent cut-off requirements of the sideband filter in the filter method of SSBSC generation are somewhat reduced for Miller encoded data signals, because there is a relatively large separation between the wanted and the unwanted sidebands after modulation. The spectrum of the modulated signal lies between $f_c \pm \frac{1}{4}R_b$ and $f_c \pm \frac{1}{2}R_b$ and there is little energy content at f_c.

In the filter method of SSBSC generation, practical implementations of the filter is done with crystal filters, which give excellent suppression of the unwanted sideband [18]. The filter method of SSBSC generation with Miller encoded information yields acceptable adjacent

sideband suppression and this method of SSBSC generation is presented in the following section.

3.2 The Filter method of SSBSC Generation

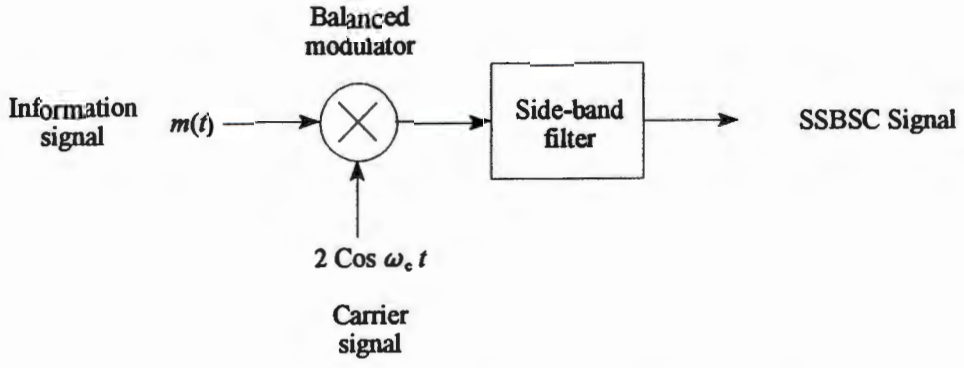

Figure 3.1: The filter method of SSBSC generation.

The first step in this modulation process is, using a balanced modulator, to multiply the information signal $m(t)$ by the carrier signal to produce a DSBSC signal. If the information signal is a sinusoidal signal represented by $m(t) = \cos(\omega_m t)$ and the carrier signal is represented by $f_c(t) = 2\cos(\omega_c t)$, then the output of the multiplier using simple trigonometry is

$$\begin{aligned} e_{DSBSC}(t) &= 2\cos(\omega_c t) \times \cos(\omega_m t) \\ &= \cos(\omega_c - \omega_m)t + \cos(\omega_c + \omega_m)t \end{aligned} \tag{3.1}$$

For this simple case, the LSB and USB are explicitly identified in equation 3.1 as the first and second terms respectively. The sideband filter now removes the unwanted sideband resulting in either the USB or LSB being transmitted. Thus the SSBSC output signal is given by

$$e_{SSBSC}(t) = \cos(\omega_c + \omega_m)t \text{ for the USB} \tag{3.2}$$

or $$e_{SSBSC}(t) = \cos(\omega_c - \omega_m)t \text{ for the LSB} \quad (3.3)$$

The double sided frequency spectrums for single tone modulation are presented in figure 3.2.

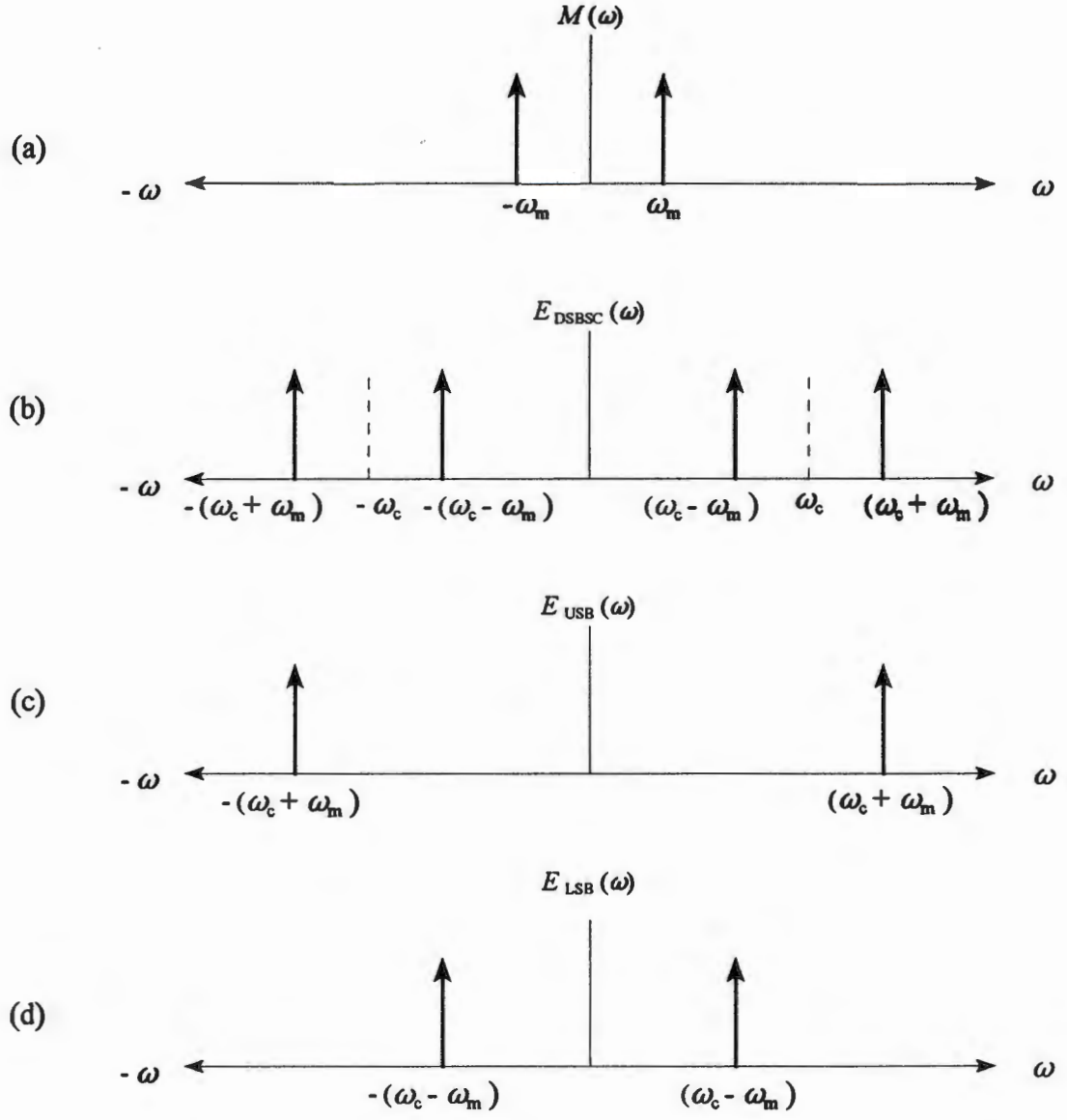

Figure 3.2: Double sided frequency spectrums for single tone SSBSC modulation.

It can be clearly seen that the spectra shown in figure 3.2 (b), 3.2 (c) and 3.2 (d) do indeed correspond to equations 3.1, 3.2 and 3.3 respectively.

3.3 VPSK Generation in the Simulation

The filter method of SSBSC generation in the simulation is implemented using the standard set of tokens available in the SystemView library.

3.3.1 Schematic of the 2-VPSK Modulator

Figure 3.3 shows the block diagram of the SSBSC modulator as implemented in the simulation, and used to generate a 2-VPSK signal.

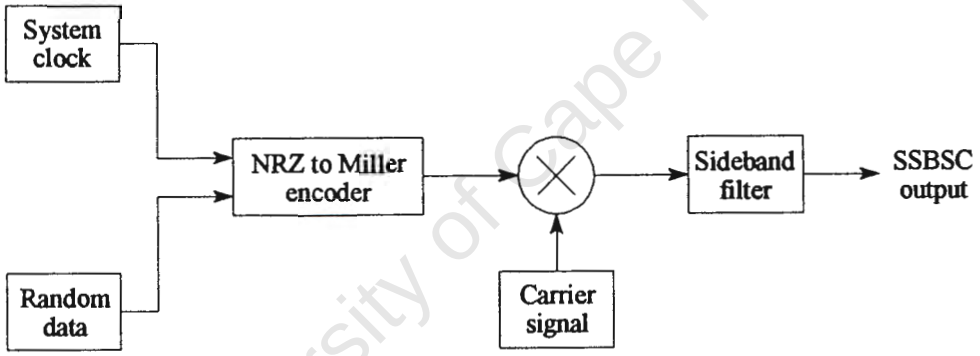

Figure 3.3: VPSK modulator as implemented in SystemView.

The bipolar Miller coded signal is applied to a two input multiplier and the sinusoidal carrier to the remaining input. The sinusoidal carrier token is selected from the source library and has an amplitude of 1 volt and a frequency of 16 Hz and an initial phase of 0 degrees. The DSBSC output of the multiplier is then applied to the bandpass filter which was implemented from the extremely powerful linear system token in the operator library.

The bandpass filter was defined as a linear phase analog bandpass filter with 3 poles and with a phase ripple of 0.05 dB. The cut-off frequencies were specified at 16 Hz and 17 Hz. The z transform transfer function of the sideband filter is given by

$$H(z) = \frac{5.59\times10^{-5} - 1.679\times10^{-4}z^{-2} + 1.679\times10^{-4}z^{-4} - 5.5969\times10^{-5}z^{-6}}{1 - 2.9z^{-1} + 5.765z^{-2} - 6.568z^{-3} + 5.442z^{-4} - 2.645z^{-5} + 0.841z^{-6}} \quad (3.4)$$

The magnitude and phase plot of the sideband filter is shown in figure 3.4

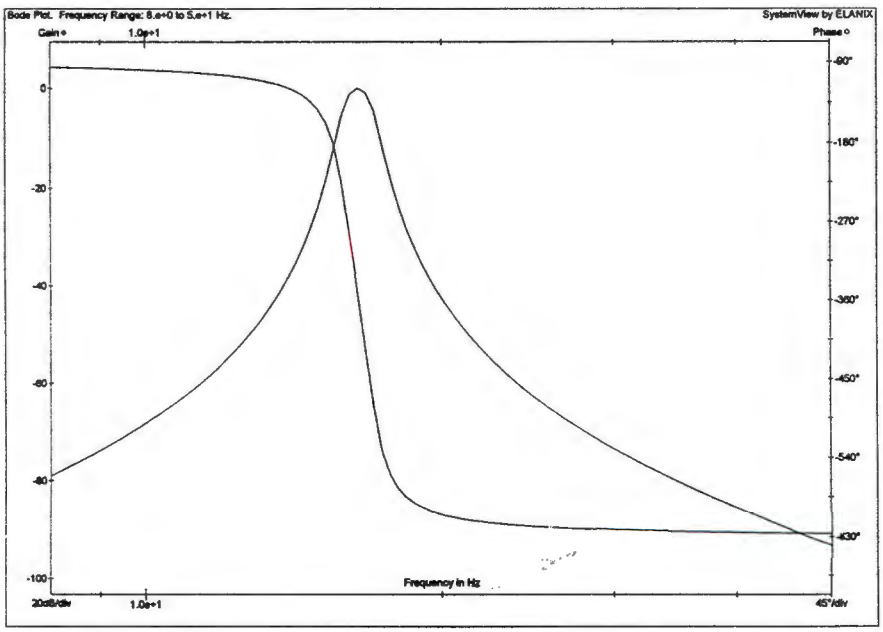

Figure 3,4: Magnitude and phase plot of the sideband filter.

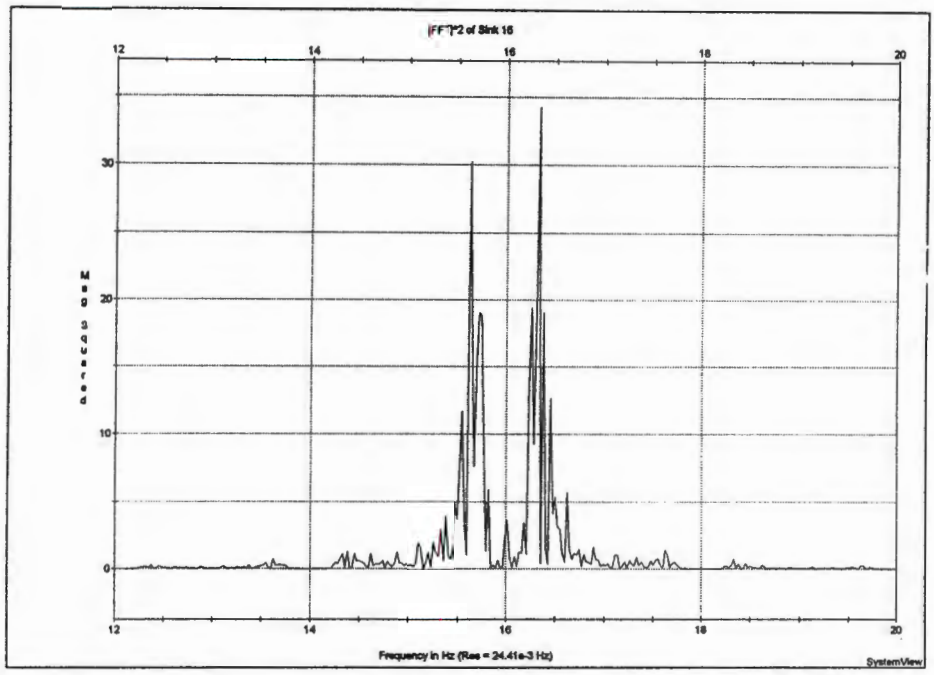

Figure 3.5: DSBSC output of multiplier in the simulation.

The DSBSC output of the multiplier is shown in figure 3.5. This figure clearly shows the Miller spectrum spaced around a suppressed carrier of 16 Hz.

Finally, the time and frequency domain representations of the 2-VPSK signal at the output of the sideband filter are shown in figures 3.6 and 3.7 respectively. In this simulation the upper sideband was selected.

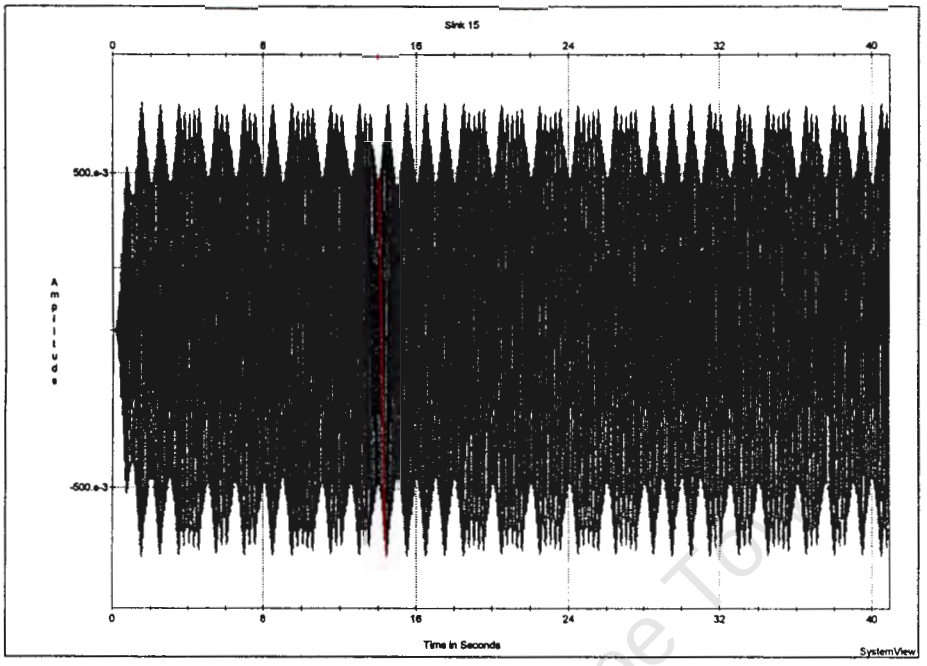

Figure 3.6: Time domain representation of a USB 2-VPSK modulated signal.

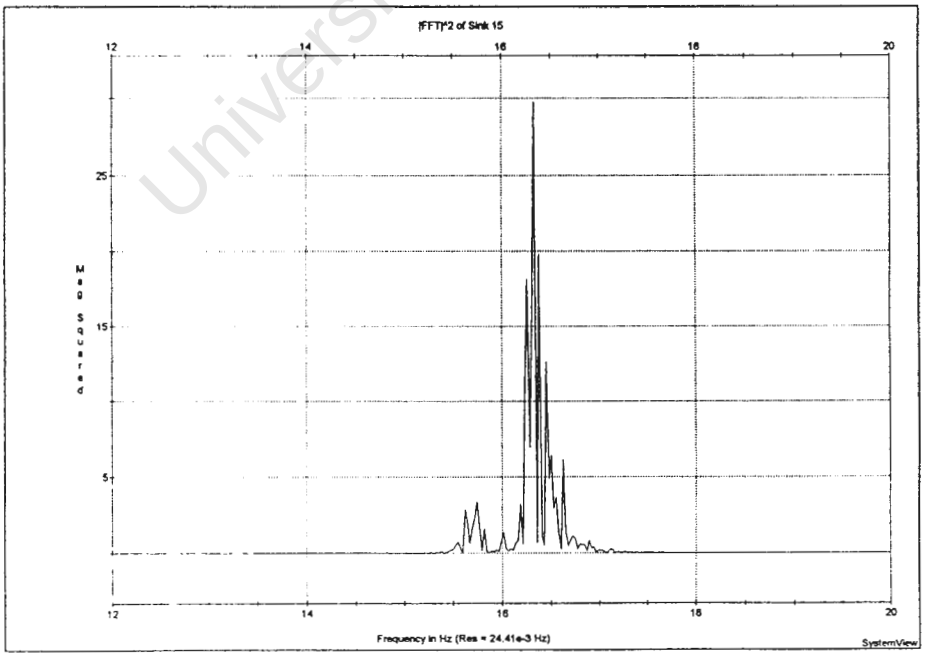

Figure 3.7: Frequency spectrum of a USB 2-VPSK modulated signal.

Chapter 4

Spreading the Spectrum of the VPSK Signal

In chapter 3 the generation of a 2-VPSK signal was presented. The VPSK signal is a SSBSC signal and thus does not have any carrier component in the passband signal. In present VPSK systems, the VPSK passband signal is translated back down to baseband by coherent demodulation in the receiver. Any frequency or phase discrepancy between the locally generated and original carrier signals will result in the failure of the demodulation process and hence performance will be severely degraded.

The approach used by Walker [2] to overcome the loss of carrier in the transmitted signal is to reference the locally generated carrier in the receiver to an integer multiple of the symbol clock frequency. His assumption is that the received carrier will be close enough to the transmitted carrier to allow carrier recovery and coherent demodulation to take place. This assumption is not valid if the channel is a noisy multi-path environment or has any significant doppler characteristics.

The main aim of this thesis is to find an alternative means, using DSSS techniques, of providing a reference for the locally generated carrier and symbol clock signals, necessary for coherent demodulation. In the transmitter, the PN chipping sequence is made a multiple of the symbol clock as is the original carrier signal. When the PN chipping signal is recovered in the receiver the locally generated carrier and symbol clock signals are derived from the oscillator in the PN code tracking loop.

In this chapter the spreading of a phase modulated carrier signal using DSSS is analysed in detail. The DSSS system as implemented in the simulation is then presented.

4.1 Direct Sequence Spread Spectrum Modulation

4.1.1 DSSS Transmitter

The simplest form of DSSS employs binary phase shift keying as the spreading modulation. BPSK modulation results in instantaneous phase changes of the carrier by 180° and can be mathematically represented as a multiplication of the carrier by a function $c(t)$ which takes on the values ± 1 [19].

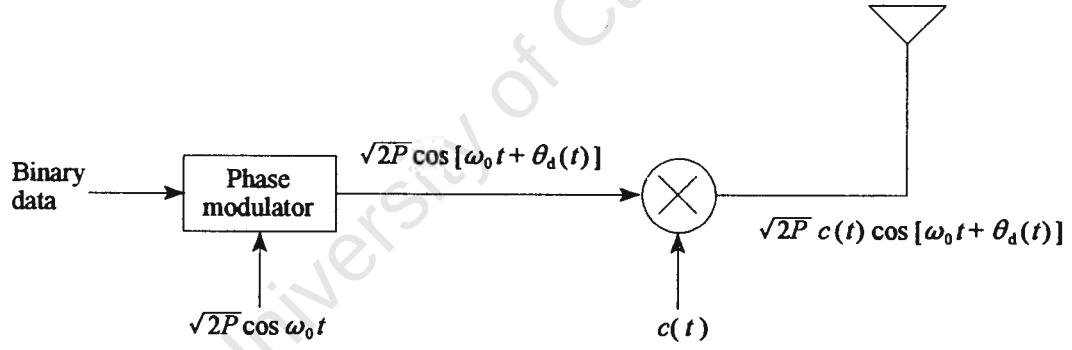

Figure 4.1: BPSK direct sequence spread spectrum transmitter [19].

The constant-envelope data modulated carrier having power P, angular frequency ω_0, and data phase modulation $\theta_d(t)$ defined by

$$S_d(t) = \sqrt{2P}\cos[\omega_0 t + \theta_d(t)] \tag{4.2}$$

This signal occupies a bandwidth typically between one-half and twice the data rate prior to spreading, depending on the details of the data modulation. BPSK spreading is accomplished by multiplying $S_d(t)$ by a function $c(t)$ which represents the spreading waveform. This is illustrated in figure 4.1. The transmitted signal is

$$S_t(t) = \sqrt{2P}\, c(t) \cos[\omega_0 t + \theta_d(t)] \tag{4.2}$$

This signal is transmitted via a distortion less path having transmission delay T_d. The signal is received together with some type of interference and/or Gaussian noise.

4.1.2 DSSS Receiver

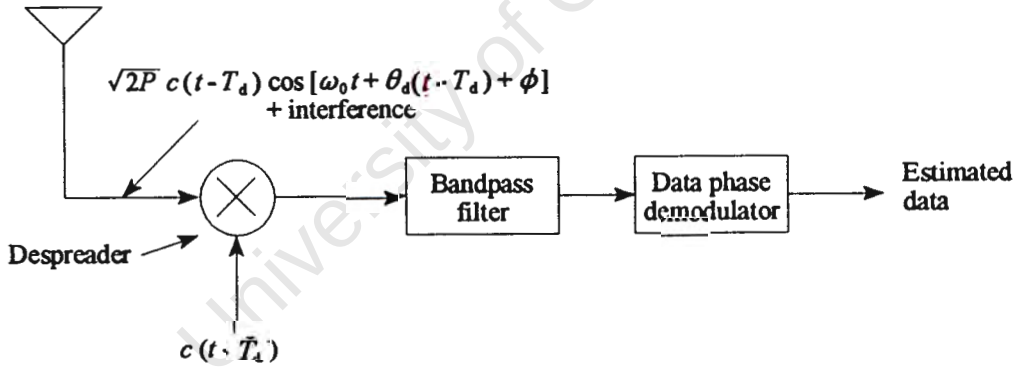

Figure 4.2: BPSK direct sequence spread spectrum receiver [19].

Demodulation is accomplished in part by despreading with the spreading code appropriately delayed as shown in figure 4.2. This despreading function is critical in all spread spectrum systems. The signal component at the output of the despreading mixer is

$$\sqrt{2P}\, c(t - T_d) c(t - \hat{T}_d) \cos[\omega_0 t + \theta_d(t - T_d) + \phi] \tag{4.3}$$

where $\hat{T}_d$ is the receiver's best estimate of the transmission delay.

Since $c(t) = \pm 1$, the product $c(t-T_d) \times c(t-\hat{T}_d) = 1$ if $\hat{T}_d = T_d$, that is, if the spreading code in the receiver is synchronised with the spreading code in the transmitter. When correctly synchronised, the signal component at the output of the de-spreading mixer is equal to $S_d(t)$ except for a random phase ϕ and $S_d(t)$ can be demodulated using a conventional coherent phase demodulator.

The data modulation does not have to be BPSK and no restrictions have to be replaced on the form of $\theta_d(t)$ [19]. However it is common to use the same type of digital phase modulation for the data and spreading code. For a comprehensive analysis of the time domain representations of the spreading and de-spreading waveforms, see Peterson, Zeimer and Borth [19].

4.1.3 Power Spectral Density of a DSSS Signal

The power spectral density in W/Hz of a BPSK carrier is given by [19][20]

$$S_d(f) = \tfrac{1}{2} P T_b \left\{ sinc^2[(f-f_0)T_b] + sinc^2[(f+f_0)T_b] \right\} \qquad (4.4)$$

and is shown in figure 4.3.

The transmitted signal represented by equation 4.2 is also a binary phase shift keyed carrier and therefore has a power spectral density which is given by equation 4.4, but with the bit period T_b replaced with T_c, which is the duration of the spreading (chipping) code symbol.

The effect of the modulation of the data modulated carrier by the chipping code is to spread

the bandwidth of the transmitted signal by a factor of T_b/T_c. Figure 4.4 shows the power spectral density of equation 4.2 in the case where $T_c = T_b/3$.

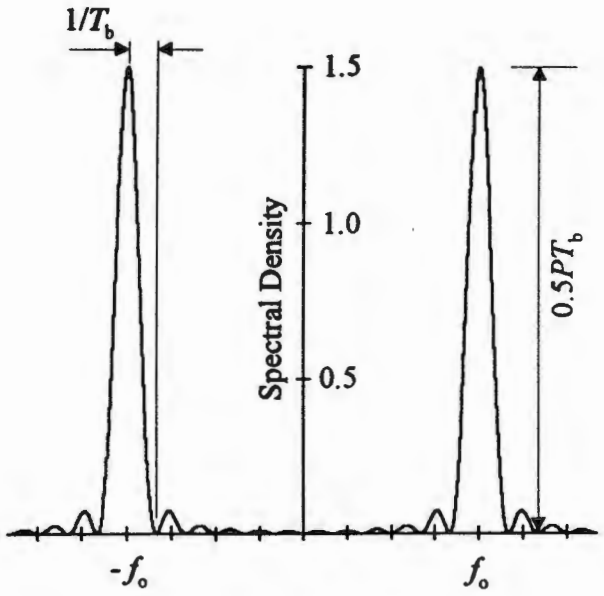

Figure 4.3: Power spectral density of a BPSK data modulated carrier [19][20].

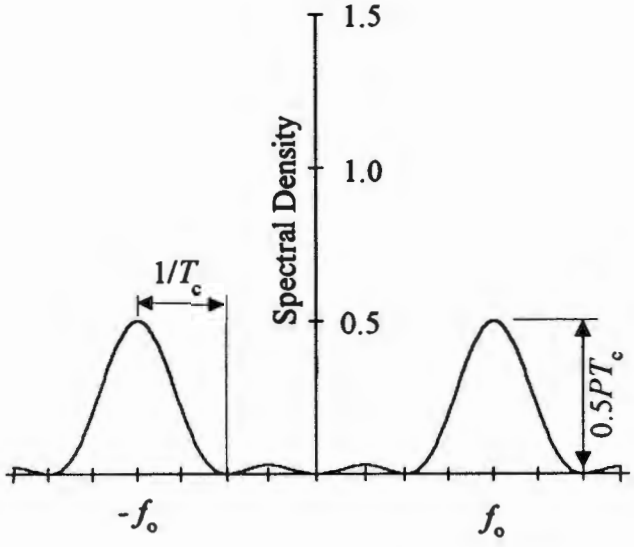

Figure 4.4: PSD of the data and spreading code modulated carrier [19].

Figure 4.4 clearly shows that the effect of the modulation by the spreading code is to spread the bandwidth of the transmitted signal by the factor T_b/T_c, which is 3 in the above case. The spreading operation also reduces the amplitude of the PSD by the same factor. In practice, this spreading factor is much larger than the factor 3 used in this example.

4.2 Pseudo-noise Sequence Generators

The waveform $c(t)$ used to spread and despread the data modulated carrier is called a PN (pseudo-noise) or pseudorandom sequence. It is a binary sequence that is deterministically generated, yet possesses properties of randomly generated sequences. Although a PN sequence is deterministic, it should have the following characteristics called randomness properties [21]:

- Balance property: in each period of the sequence, the number of 0's and 1's differ by at most one digit.

- Run property: A run is defined as a sequence of a single type of binary digit. The appearance of another digit in a sequence starts a new run. The length of a run is the number of digits in that run. Among the runs of 1's and 0's in each period of a PN sequence, it is desirable that about one-half the runs of each type are of length 1, about one-quarter are of length 2, one-eight are of length 3, and so on.

- Correlation property: If a period of a sequence is compared term by term with any cyclic shift of itself, it is best if the number of agreements differs from the number of disagreements by not more than one count.

Auto-correlation is the integral of the complex inner product of the sequence with a shifted version of itself and is a measure of the similarity between a signal $x(t)$ and a τ-second time shifted replica of itself. The auto-correlation function of a periodic waveform $x(t)$, with

period T_0 is defined in normalised form by [21]

$$R_{xx}(\tau) = \frac{1}{K}\left(\frac{1}{T_0}\right)\int_{-T_0/2}^{T_0/2} x(t)\cdot x(t-\tau)\,dt \qquad \text{for } -\infty < \tau < \infty \tag{4.5}$$

where

$$K = \frac{1}{T_0}\int_{-T_0/2}^{T_0/2} x^2(t)\,dt \tag{4.6}$$

When $x(t)$ is a periodic waveform representing a PN code, each fundamental pulse is referred to as a code symbol or a chip. For such a PN waveform of unit chip duration and period p chips, the normalised auto-correlation function may be expressed as

$$R_{xx}(\tau) = \frac{1}{p}\cdot\left(\begin{array}{l}\text{number of agreements less number of disagreements}\\ \text{in a comparison of one full period of the sequence}\\ \text{with a } \tau \text{ position cyclic shift of the sequence}\end{array}\right) \tag{4.7}$$

and shown figure 4.5.

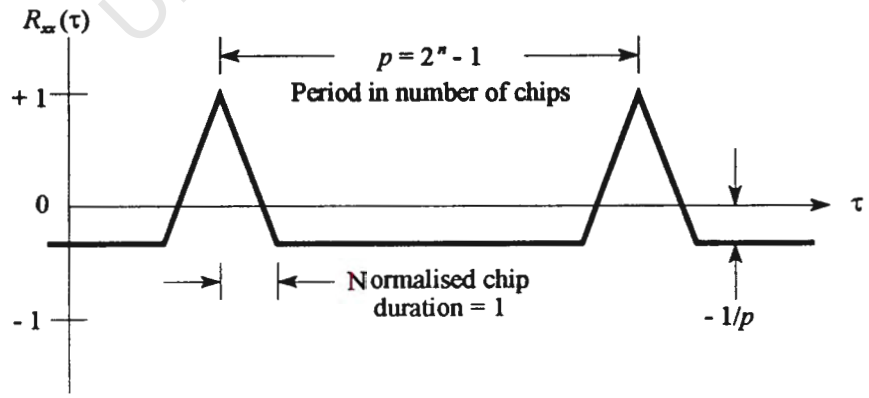

Figure 4.5: Normalised auto-correlation function for a maximal length sequence [21].

When $x(t)$ and its replica are perfectly matched, that is when $\tau = 0$, then $R_{xx}(\tau) = 1$. For any cyclic shift between $x(t)$ and $x(t + \tau)$ with $(1 \leq \tau \leq p)$, the auto-correlation function is equal to $-1/p$. For a large p the sequences are virtually de-correlated for a shift of a single chip.

The PN sequence is usually generated using a sequential logic feedback shift register, a block diagram of which is shown in figure 4.6.

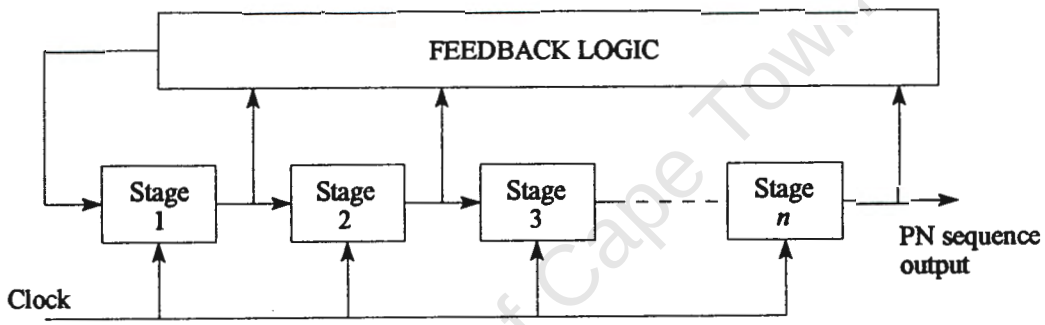

Figure 4.6: Generalised feedback shift register with n stages.

The feedback shift register consists of consecutive two state memory devices and feedback logic. Binary sequences are shifted through the shift registers in response to clock pulses, and the output of the various stages are logically combined and fed back as the input to the first stage. When the feedback logic consists of exclusive-OR gates, which is usually the case, the shift register is called a linear PN sequence generator [21].

The initial contents of the memory stages and the feedback logic circuit determine the successive contents of the memory. Since there are exactly $2^n - 1$ non-zero states for an n-stage feedback shift register, the period of a PN sequence produced by a linear n-stage shift register cannot exceed $2^n - 1$ symbols. A sequence of period $2^n - 1$ generated by a linear feedback register is called a maximal length sequence.

4.3 The Performance of a DSSS System

One of the advantages of SS (spread spectrum) systems is the ability of these systems to reject interference that otherwise might prohibit useful communications. However, thermal noise is not rejected by SS techniques [23]. In this section a heuristic demonstration and physical interpretation of the performance of SS systems is presented. A more comprehensive treatment is presented in Rappaport [22] or Peterson, Ziemer and Borth [19].

From figure 4.1 it is clear that the spectral spreading is achieved by the modulating the BPSK signal, which has instantaneous signal-state changes between +1 and -1 at a rate of $f_b = 1/T_b$, with a PN spreading signal $c(t)$, which has instantaneous voltage changes between +1 and -1 at a chip rate of $R_c = f_c = 1/T_c$. In the overall SS systems, the baseband data signal is twice multiplied by the spreading-despreading PN sequence. Since $c^2(t) = 1$, as $1^2 = 1$ and $(-1)^2 = 1$, there is no effect on the received despread output signal.

Thermal noise or AWGN (additive white Gaussian noise) is introduced in the receiver by the front end amplifiers and converters, which have a noise bandwidth at least as wide as the SS signal. During the despreading process this noise is multiplied by the despreading PN sequence. Multiplication reverses the polarity of the noise waveform at nominally random times at integer multiples of the chip duration T_c [23]. Polarity reversal has no impact on the PSD or the PDF (probability density function) of the AWGN.

Thus the spreading-despreading process does not affect either the signal or the spectral and probability density functions of the noise, and the overall BER (bit error rate) or probability of error, P_e, performance of a SS system in an AWGN-controlled channel is the same as the performance of the modulated system without SS [23].

In the case of a coherent BPSK SS system, the probability of error is given by

$$P_e = Q\left[\sqrt{\frac{2E_b}{N_0}}\right] \tag{4.8}$$

where $E_b = A^2T_b$ = the average energy of a received bit

A^2 = the average power of the received carrier

N_0 = noise density = noise power in 1 Hz of RF bandwidth

T_b = bit period

However, if the channel has intentional narrowband or wideband interference called jamming, then SS systems have excellent rejection capabilities. The error performance for a SS system under these conditions is given by [23]

$$P_e = Q\left[\sqrt{2\left(\frac{P_s}{P_J}\right)\left(\frac{f_c}{f_b}\right)}\right] \tag{4.9}$$

where P_s = the received, desired signal power at the receiver RF input

P_J = the power of the interfering signal at the receiver RF input

f_c = the chipping rate = $1/T_c$

f_b = the bit rate = $1/T_b$

The quantity

$$P_{J_{eff}} = \frac{P_J}{2(f_c/f_b)} \tag{4.10}$$

is known as the effective jamming power, and in comparison with the signal power P_s, determines the performance of the SS system.

The chipping-rate to bit-rate ratio, f_c/f_b, determines the reduction of the narrow- or wideband interference power, and is defined as the processing gain $G_p = f_c/f_b$.

It is thus clear that, for wide- or narrowband interference, the performance of a SS system is determined by the choice of the chipping frequency. The higher the ratio of chip rate to bit rate the better the BER performance of the system.

4.4 DSSS Transmitter in the Simulation

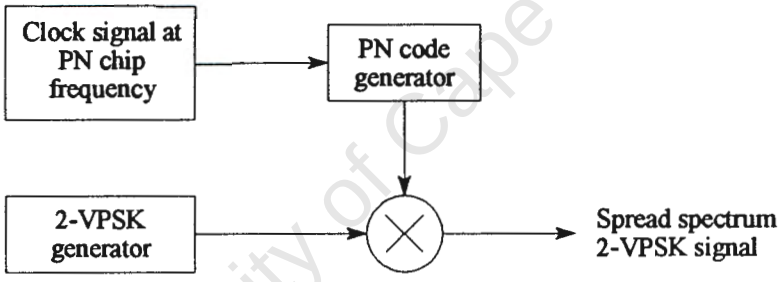

Figure 4.7: DSSS transmitter as implemented in the SystemView simulation.

Figure 4.7 shows how the spectrum of the VPSK signal is spread. A multiplier token multiplies the output of the sideband filter, the VPSK signal, with a PN sequence derived from a PN sequence generator token selected from the communications library. The PN sequence parameters were selected as

- register length: 12
- seed: -1
- chip rate: 8 Hz

This gives a sequence length of 2^{12} - 1 which clearly is a maximal length PN sequence.

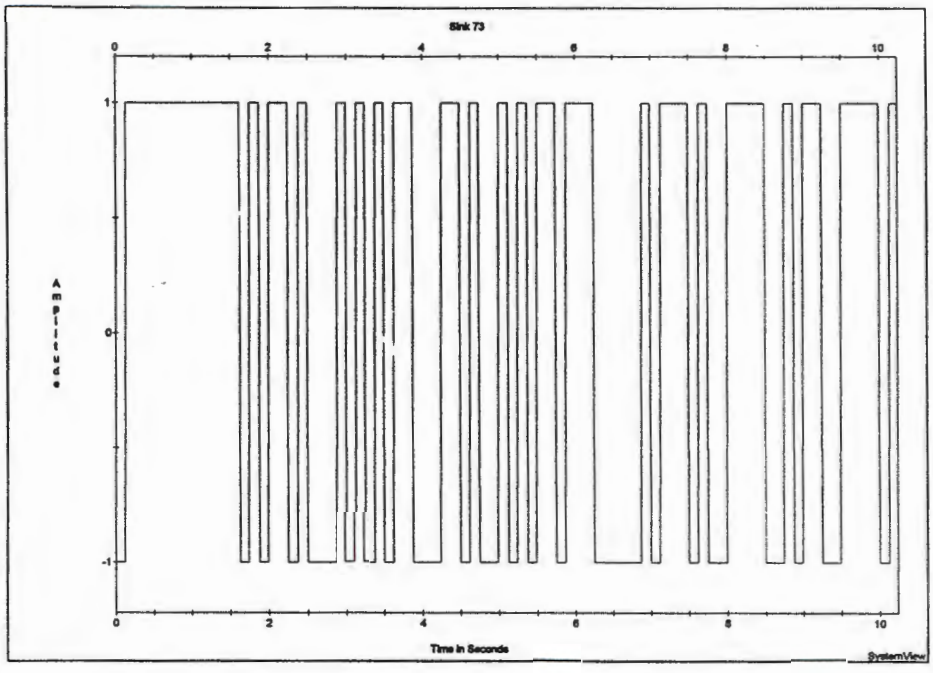

Figure 4.8: PN sequence waveform generated in SystemView.

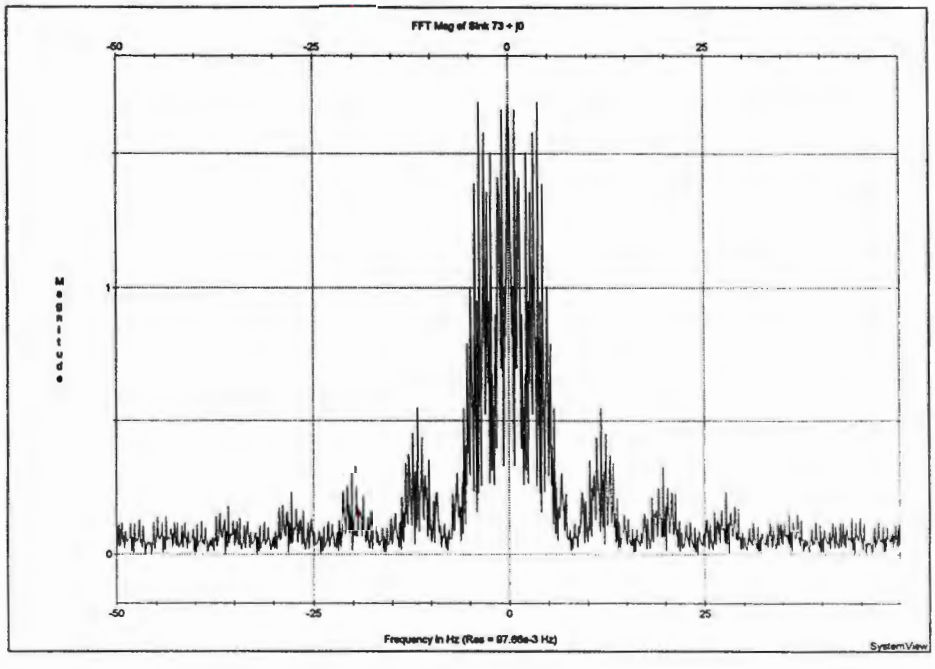

Figure 4.9: Double sided spectrum of the PN code.

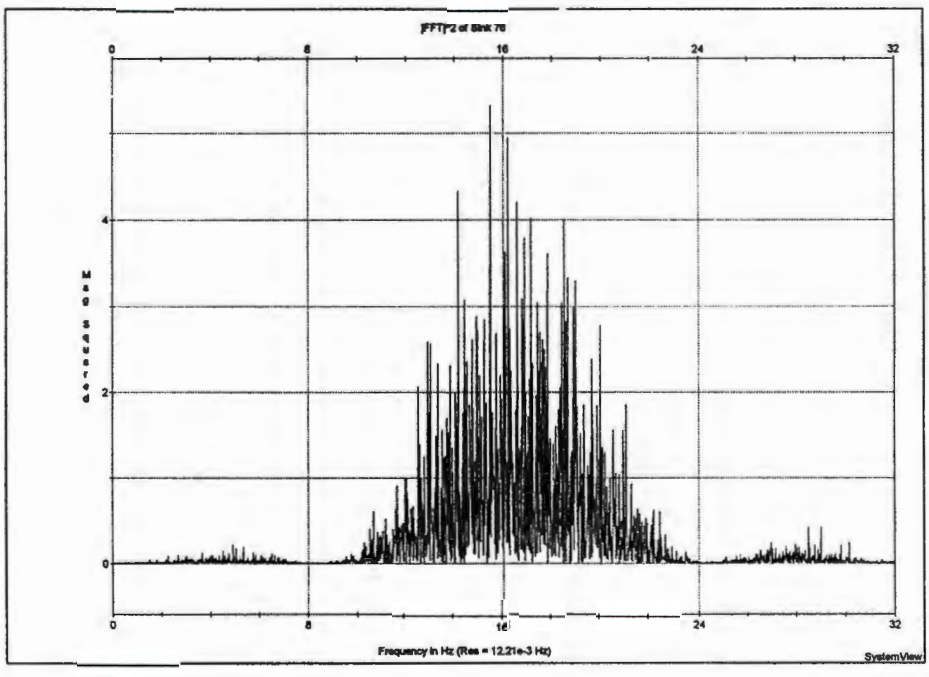

Figure 4.10: Power spectrum of the spread VPSK signal.

Chapter 5

The Channel

All communication systems contain a channel. Generally, the channel represents the transmission media and the receiver front end, which usually means down to the first mixer. The transmission media is the propagating medium or electromagnetic path connecting the transmitter and the receiver. The transmission media might consist of copper wires, coaxial cables, fibre optic cables, and in the case of RF (radio frequency) links, the atmosphere or empty space. All channels have a maximum and minimum frequency cut-off, beyond which input components are almost entirely attenuated.

A channel acts partly as a filter, to attenuate and distort the signal propagating through the channel. Distortion can be linear or non-linear and this distortion can be corrected to some degree by the receiver. In addition to this distortion encountered in the channel, the propagating signal is also contaminated by undesirable signals, lumped under the broad term noise, and which are random unpredictable signals from causes internal and external to the communications system.

Examples of external noise are:

- Signals transmitted on adjacent channels
- man-made noise such as that radiated from flourescent lights, arc-welders etc.
- natural noise from lightning, electrical storms and solar radiation

Much of the unwanted external signal distortion can be reduced or eradicated by careful system design. However, no matter how good the system design is, there is a natural form of internal distortion that is always prevalent, called thermal or Johnson noise [21] and it is described as a zero-mean Gaussian random process. Proper design can minimise the effects of internal noise but can never eliminate it. Noise is one of the basic factors that sets a limit on the rate of communication.

Since thermal noise is present in all communication systems and is the prominent noise source for most systems, the thermal noise characteristics - additive, white, and Gaussian - are often used to model the noise in communication systems. Since zero-mean Gaussian noise is completely described by its variance, this model is particularly simple to use in the detection of signals and is presented in the following section.

5.1 The Additive White Gaussian Noise Channel

The primary spectral characteristic of thermal noise is that its PSD is the same for all frequencies of interest. This means that a thermal noise source generates an equal amount of noise power per unit bandwidth at all frequencies - from d.c. to about 10^{13} Hz [6][21]. Therefore, a simple model for thermal noise assumes that its PSD, $G_n(f)$, is flat for all frequencies, as shown in figure 5.1 (a), and denoted by [21]:

$$G_n(f) = \frac{N_0}{2} \quad \text{watts/hertz} \tag{5.1}$$

The factor 2 indicates that $G_n(f)$ is a two-sided power spectral density. When the noise power has such a uniform spectral density, it is referred to as white noise and adds an equal amount of noise power per unit bandwidth at all frequencies.

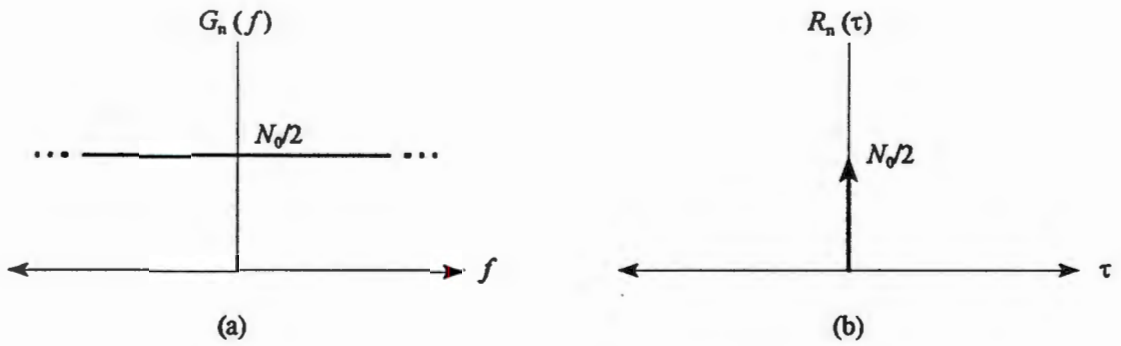

Figure 5.1: (a) PSD of white noise. (b) Auto-correlation function of white noise.

The auto-correlation function of white noise is given by the inverse Fourier transform of the noise PSD in equation 5.1, and is denoted as [21]:

$$R_n(\tau) = \mathcal{F}^{-1}\{G_n(f)\} = \frac{N_0}{2}\delta(\tau) \tag{5.2}$$

The auto-correlation function of white noise is a Dirac delta function weighted by the factor $N_0/2$ and occurring at $\tau = 0$, as shown in figure 5.1 (b). Since $R_n(\tau)$ is zero for $\tau \neq 0$, any two different samples of white noise, no matter how close together in time they are taken, are uncorrelated.

Therefore, the effect on the detection process of a channel with AWGN is that the noise affects each transmitted symbol independently. Such a channel is called a memoryless channel. The term additive means that the noise is superimposed or added to the signal and there are no multiplicative mechanisms involved.

5.2 The AWGN Channel as implemented in the Simulation

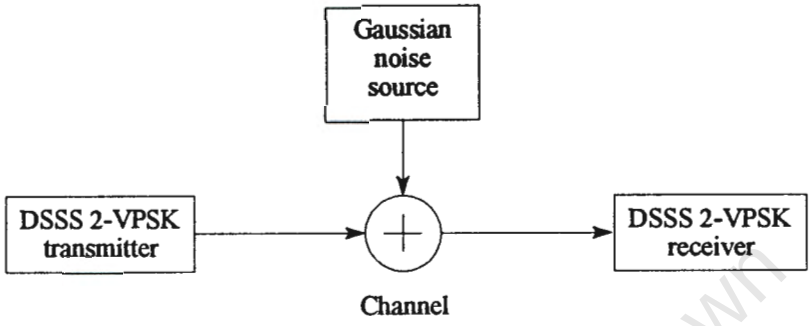

Figure 5.2: The AWGN channel model as implemented in SystemView.

The Channel as implemented in the simulation consists of a multiple input adder token, which forms the sums of its inputs, and a Gaussian noise token from the source library. This Gaussian noise source token generates a random signal with a Gaussian (normal) distribution. The user defined parameters are as follows:

- Standard deviation or PSD in W/Hz
- mean

Figure 5.3 shows an example of the noise signal generated by the Gaussian noise source.

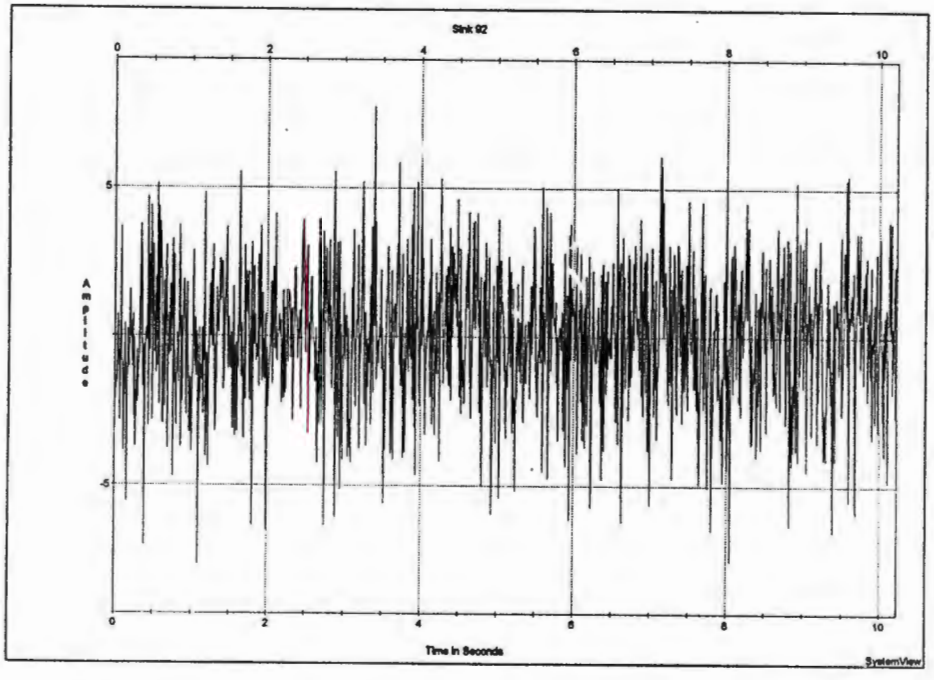

Figure 5.3: AWGN signal produced by noise source in the simulation.

The AWGN source provides a real valued output and does not introduce any phase distortion, as could be the case in a practical application. Any kind of phase corruption would severely distort a VPSK signal because the digital information is phase shift keyed and also since it is a SSBSC system, there is only one sideband, thus even less phase information.

Chapter 6

Despreading the Spread Spectrum VPSK Signal

Spread spectrum communication requires that the transmitter and the receiver spreading waveforms be synchronised. If the two waveforms are out of synchronisation by as little as one chip, insufficient signal energy will reach the receiver data demodulator for reliable detection [19]. The task of acquiring and maintaining code synchronisation is delegated to the receiver.

6.1 Spread Spectrum Synchronisation

Synchronisation of the PN code spreading sequence is by far the most complicated process in the overall spread spectrum system. Many texts assume perfect PN code synchronisation between transmitter and receiver when analysing spread spectrum systems. Dixon [7] puts this assumption into perspective by stating,

"What an assumption! More time, money and effort has been spent on developing and improving synchronisation techniques than in any other area of spread spectrum systems. There is no reason to suspect that this will not continue to be true in the future."

Synchronisation of a PN code in a spread spectrum receiver is accomplished in two stages. First the initial coarse synchronisation (acquisition) is performed and then PN code tracking is maintained. As the emphasis in this thesis is on investigating an alternative method of carrier synchronisation for coherent data demodulation of VPSK, only PN code tracking was implemented in the simulation, thus the method used for PN code tracking will be presented. It is assumed that code acquisition is complete and that the transmitted and received sequences are within one chip.

6.2 PN Code Tracking

Once initial synchronisation has been achieved, that is, the transmitted and locally generated receiver PN sequence code-phase are less than one chip apart, code tracking loops are used to complete the synchronisation by accurately locking and maintaining lock.

Code tracking is accomplished by using phase-locked loop techniques, and correlation operations between the received signal and two different phases, early and late, of the receiver-generated spreading waveform. Tracking code loops are classified as coherent or non-coherent. If the carrier frequency and phase are known exactly, a coherent loop or baseband loop can be used. However, when no a priori carrier frequency and phase information is known, as would be the case for a doppler channel, then non-coherent code tracking loops are used. Tracking loops are further classified as:

- a full time early-late tracking loop, often referred to as a delay-locked loop
- a time-shared early-late tracking loop, often referred to as a tau-dither loop

In this thesis a non-coherent full-time delay-locked tracking loop is used and is presented in the following section.

6.2.1 Non-coherent Full-time Delay-locked Code Tracking loop

The block diagram of a basic non-coherent full-time delay-locked code tracking loop for a direct sequence spread spectrum system using BPSK is shown in figure 6.1 [21].

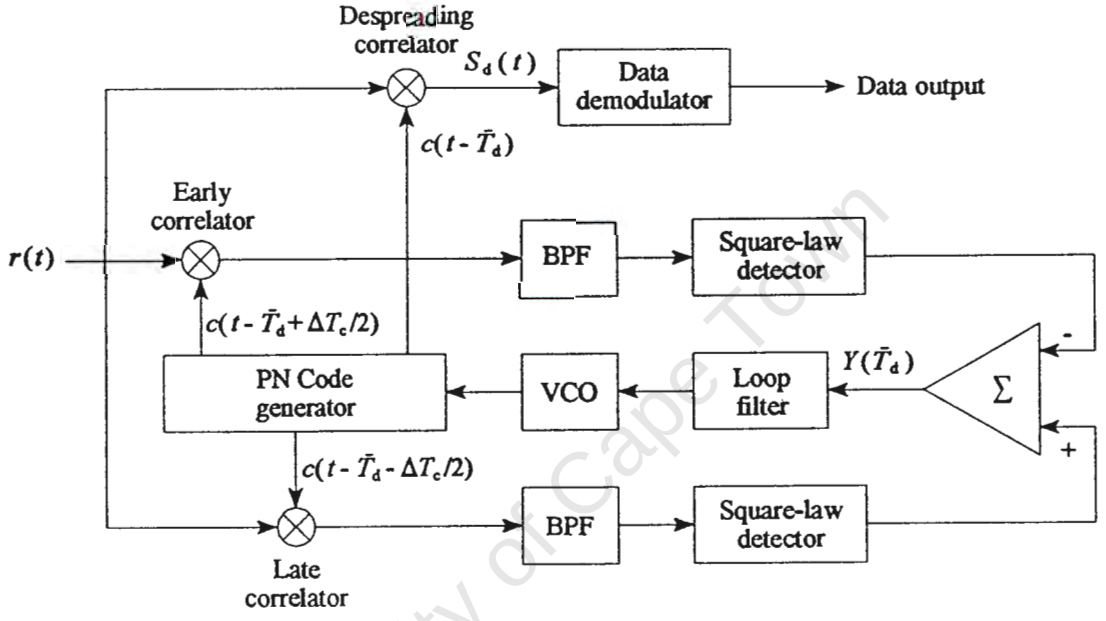

Figure 6.1: Non-coherent full-time delay-locked code tracking loop.

The non-coherent delay-locked loop employs a phase discriminator, a loop filter, a voltage controlled oscillator and a spreading PN code generator. The phase discriminator contains two energy detectors which are not sensitive to data modulation or carrier phase, and thus enable the discriminator to ignore data modulation and carrier phase [19].

A linear equivalent circuit for the full-time delay-locked PN code tracking loop is presented in figure 6.2 to illustrate the resemblance to a standard PLL (phase-locked loop) [19].

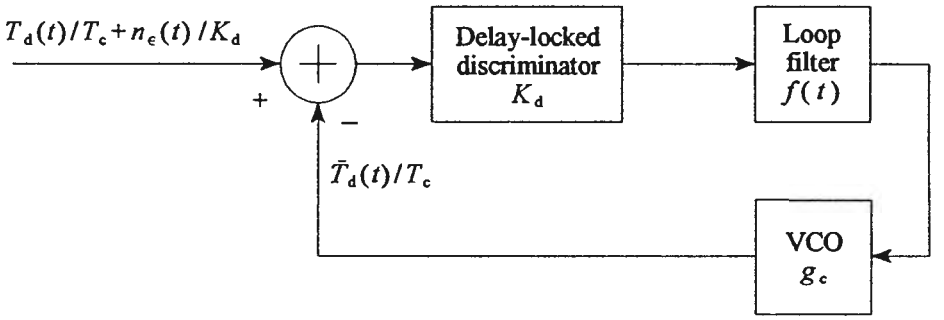

Figure 6.2: Linear equivalent circuit for the full-time early-late non-coherent delay-locked code tracking loop.

where:

g_c = VCO gain in Hz/volt

$K_d = \left(1 + \frac{1}{N}\right)\left[1 - \left(1 + \frac{1}{N}\right)\frac{\Delta}{2}\right](2K_1 P)$

K_1 = mixer conversion gain

Δ = normalised difference between early and late correlator channels

N = m-sequence spreading code period

P = received signal power

T_c = spreading waveform chip period

$n_\epsilon(t)$ = low-pass AWGN component at the discriminator output

The closed-loop transfer function $H(s)$ is given by [19]:

$$H(s) = \frac{K_d g_c F(s)}{s + K_d g_c F(s)} = \frac{\bar{T}_d(s)}{T_d(s)} \tag{6.1}$$

and the Laplace transform of the tracking error is given by [19]:

$$\frac{T_d(s) - \bar{T}_d(s)}{T_c} = \frac{T_d(s)}{T_c}\left[\frac{s}{s + K_d g_c F(s)}\right] \tag{6.2}$$

Referring to figure 6.1, the received signal $r(t)$ is, in this case, a data and spreading code modulated carrier contaminated by AWGN and is given by [19]

$$r(t) = \sqrt{2P}c(t - T_d)\cos[\omega_0 t + \theta_d(t - T_d) + \phi] + n(t) \tag{6.3}$$

where:

P is the received signal power

$\theta_d(t - T_d)$ is the arbitrary data phase modulation

T_d is the transmission delay

ϕ is the random received carrier phase

ω_0 is the carrier radian frequency

$n(t)$ represents the zero-mean white Gaussian noise process

The loop PN code generator generates two PN codes, delayed from each other by one chip period. These two code are referred to as the early and the late PN codes, and are represented by

$$c\left(t - \bar{T}_d + \frac{\Delta T_c}{2}\right) \quad \text{for the early code.} \tag{6.4}$$

and

$$c\left(t - \bar{T}_d - \frac{\Delta T_c}{2}\right) \quad \text{for the late code.} \tag{6.5}$$

These early and late PN codes are correlated by the early and late correlators respectively. The two bandpass filters pass the data and average the product of $r(t)$ and the locally generated early and late PN codes. The square-law envelope detector eliminates the data since $|S_d(t)| = 1$, that is, the magnitude of data modulated signal is 1. The output of each envelope detector is given approximately by [21]:

$$E_d \approx E\left[\left|c(t)c\left(t - \bar{T}_d \pm \frac{\Delta T_c}{2}\right)\right|\right] = \left|R_{cc}\left(\bar{T}_d \pm \frac{\Delta T_c}{2}\right)\right| \tag{6.6}$$

where

the operator $E[\cdot]$ means the expected value

$R_{cc}(\tau)$ is the autocorrelation function of the PN waveform

$\hat{T}_d$ is the receiver's best estimate of the transmission delay

When $\hat{T}_d$ is positive, the feedback signal $Y(\hat{T}_d)$ causes the voltage controlled oscillator to increase its frequency, thereby forcing $\hat{T}_d$ to decrease. When $\hat{T}_d$ is negative, $Y(\hat{T}_d)$ causes the voltage controlled oscillator to increase its frequency, thereby forcing $\hat{T}_d$ to increase. When $\hat{T}_d$ is a suitably small number, $c(t-T_d)\,c(t-\hat{T}_d) \approx 1$, yielding the despread signal $S_d(t)$, which is then applied to the data demodulator. For a more detailed analysis of the non-coherent full-time delay-locked code tracking loop see Peterson, Ziemer and Borth [19].

The disadvantage of the non-coherent delay-locked loop is that the early and late channels must be precisely gain balanced. If the early and late channels are unbalanced, the feedback signal $Y(\hat{T}_d)$ will be off-set and will not produce a zero signal when there is zero phase error between the local and receiver PN code. This balance problem was solved by a time-shared tracking loop called the non-coherent tau-dither PN code tracking loop. For a detailed analysis of this tau-dither code tracking loop see Peterson, Ziemer and Borth [19].

6.3 PN code tracking in the Simulation

The block diagram of the delay-locked PN code tracking loop in the simulation is shown in figure 6.3. Again, the delay-locked PN code tracking loop was designed using the standard tokens available in SystemView. Standard multipliers were used to multiply the received spread spectrum signal with the locally generated early and late PN codes. As the PN generator tokens cannot be accessed in SystenView, the code delay was implemented using a non-interpolating delay token from the operator library and set to within one chip period.

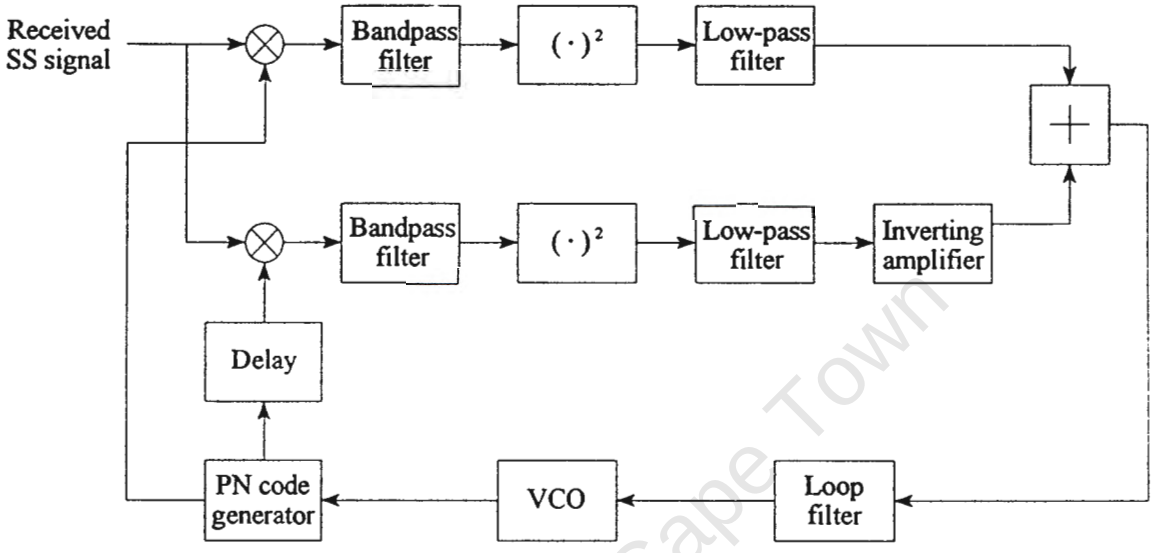

Figure 6.3: Block diagram of the delay-locked PN code tracking loop in the simulation.

The data modulated signal, that is, the difference signal at the output of the multipliers, was then selected using 8 pole IIR Butterworth bandpass filters designed from the filter library within the extremely powerful linear operator token. The bandwidth of these band pass filters must be just wide enough to pass the data-modulated signal [19], and was set to select only the data-modulated signal centred at 16 Hz.

The magnitude response of these filters is shown in figure 6.4.

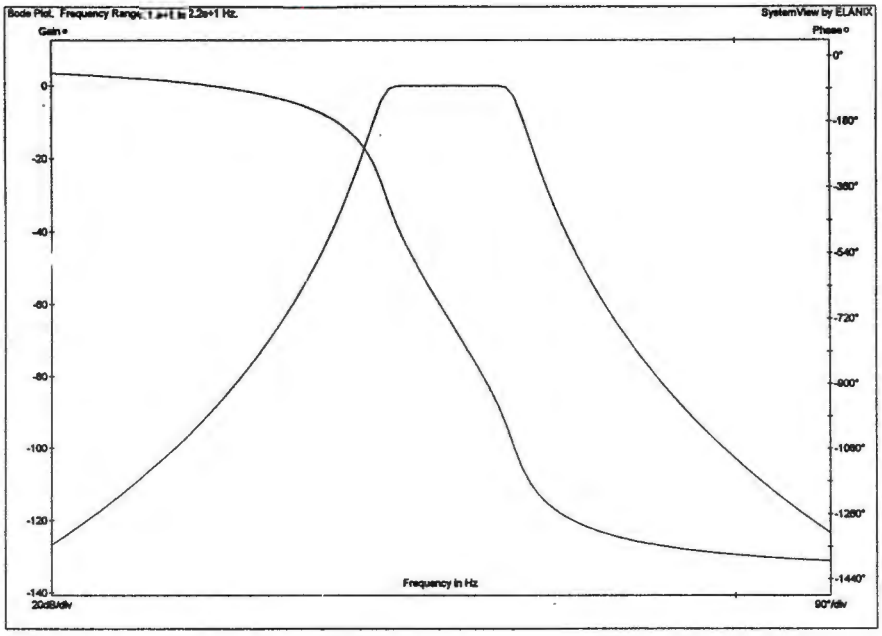

Figure 6.4: Magnitude and phase response of an 8-pole IIR bandpass filter.

The narrow-band data signal selected by the bandpass filter is applied to the square-law detector. The square-law detector was implemented by using a standard squaring token available in the SystemView functions library. The token allows the user to set the exponent of the token, which was set to 2 for squaring. Squaring this narrow-band data signal produces a component at baseband and higher harmonic components, which are then removed by the low-pass filter following the squarer, leaving only a low frequency baseband component.

The low-pass filters were implemented as low-pass Butterworth filters, selected from the analog filter library within the linear operator token in SystemView. The filter parameters were set as:

- number of poles = 3
- low frequency cut-off = 1 Hz
- filter input sample rate = 100 Hz

The sum of the early and late channels, implemented by adding the respective energy components of each channel using an adder token, is then applied to the loop filter.

The design of the loop filter is crucial to the operation of the delay-locked loop, as its behaviour determines the loop stability and dynamic behaviour of the whole code tracking loop. To improve the response of the loop, lead-lag compensation is used [19][24]. This allows the control of all the loop parameters, that is, the loop gain, the damping factor and the loop bandwidth. The loop filter in this simulation was designed using the linear operator system token with the DSP mode disabled. A custom Laplace design was used for this tracking filter, resulting in a simple lead-lag filter with a transfer function given by

$$F(s) = \frac{1 + \tau_2 s}{\tau_1 s} \tag{6.7}$$

With this loop filter, the transfer function of (6.1) becomes [19]:

$$\begin{aligned} H(s) &= \frac{[K_d g_c(\tau_2/\tau_1)]s + K_d g_c/\tau_1}{s^2 + [K_d g_c(\tau_2/\tau_1)]s + K_d g_c/\tau_1} \\ &= \frac{2\zeta\omega_n s + \omega_n^2}{s^2 + 2\zeta\omega_n s + \omega_n^2} \end{aligned} \tag{6.8}$$

where the natural loop frequency is defined by

$$\omega_n = \sqrt{\frac{K_d g_c}{\tau_1}} \tag{6.9}$$

and the damping factor is defined by

$$\zeta = \frac{\tau_2}{2}\omega_n \tag{6.10}$$

The design of the loop filter involves selecting the optimum damping factor ζ, which is usually about 0.707, so that there is minimum overshoot and a fast response time. The selection of the damping factor ζ is done in the filter design window of the linear operator system token in SystemView. The bode plot of this loop filter is shown in figure 6.5.

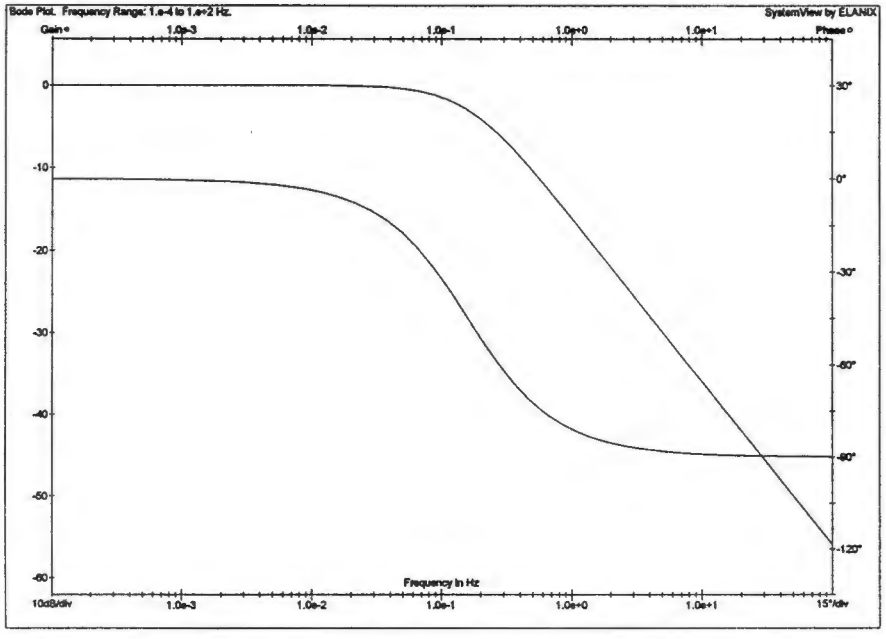

Figure 6.5: Bode plot of loop filter.

The VCO in the simulation was implemented by using the FM token from the function token library. The parameters of this VCO token were set as follows:

- amplitude = 1 V
- frequency = 8 Hz
- phase = 0 degrees
- VCO gain g_c = 0.1 Hz/volt

Finally the local PN sequence generator was implemented using the same token as that used in the transmitter. The PN generator token was selected from the communications library and

set with the same initial parameters as that in the transmitter.

The overall operation of this PN code tracking loop is verified by inspecting the cross-correlation function of the locally generated PN sequence and the original spreading PN sequence generated in the transmitter. The cross-correlation function of the original and locally generated PN sequences is shown in figure 6.6, and is generated from within the analysis window in SystemView.

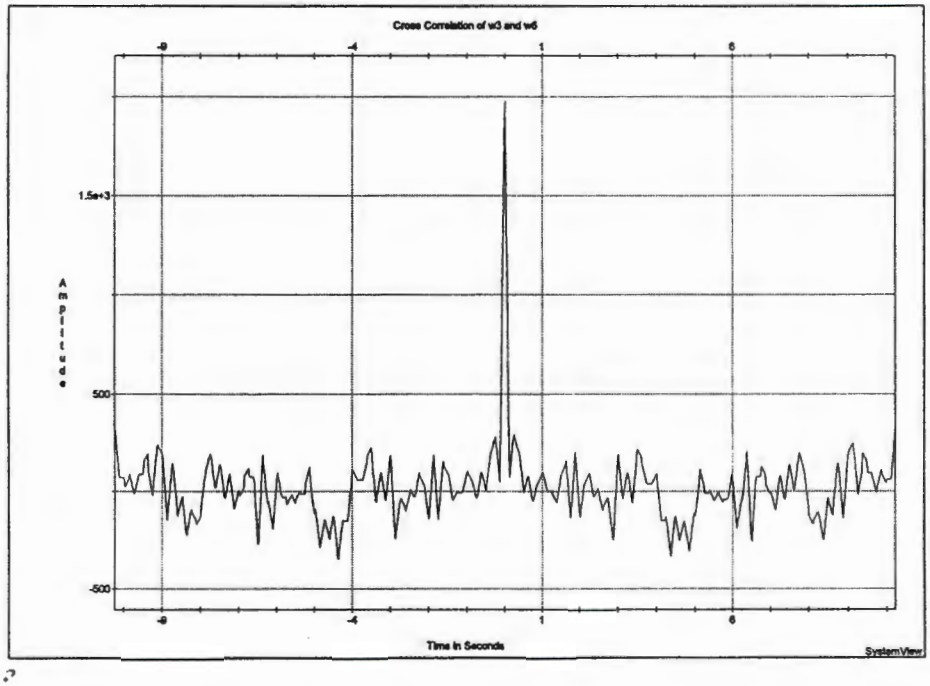

Figure 6.6: Cross-correlation of the locally generated and original PN code sequences.

It is clear from the cross-correlation function that perfect PN code synchronisation has been achieved in the simulation.

The locally generated PN code is now multiplied with the received data and code modulated signal, which is corrupted by AWGN, using a multiplier token. The resulting despread VPSK signal is shown in figure 6.7.

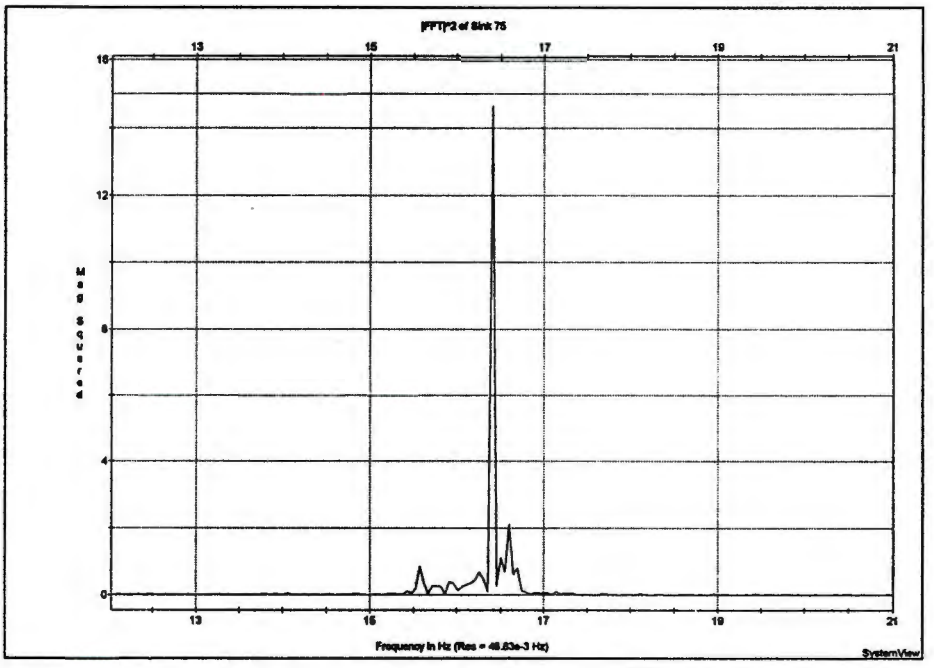

Figure 6.7: Power spectrum of the despread VPSK signal.

Chapter 7

Demodulation of Single Sideband Suppressed Carrier Signals

In chapter 6 the method of despreading the spread spectrum VPSK signal was presented and discussed with the aid of simulated results. In the despreading process it is essential that the locally generated PN code sequence is an exact synchronised replica of the original one in the transmitter. If there is more than half a chip of phase error between the original and the locally generated PN code sequence, the correlation of these codes tends to zero as shown in figure 4.5, and optimum despreading will not be accomplished, resulting in lost information. Similar stringent phase requirements, for the locally generated carrier and the original carrier signals, are necessary for proper translation of the despread VPSK signal, back down to baseband.

The purpose of this dissertation, is to investigate the viability of using the locally generated chip clock signal in the code tracking loop as the reference for the locally generated carrier, which is to be used for coherent demodulation of the VPSK signal back down to baseband.

7.1 Coherent Demodulation of SSBSC Signals

To recover the modulating signal $m(t)$ from the SSBSC signal, the spectral density of the modulated signal, that is, either the upper or lower sideband, must be translated back down

to baseband. The modulating signal $m(t)$, can be uniquely recovered from a SSBSC signal $e_{SSBSC}(t)$, by first multiplying $e_{SSBSC}(t)$ with a locally generated sinusoidal signal represented by $2\cos(\omega_c t + \theta)$, which is an exact replica of the original carrier signal in the transmitter, and then low-pass filtering the multiplier output. This process is called coherent or synchronous demodulation and is illustrated in figure 7.1.

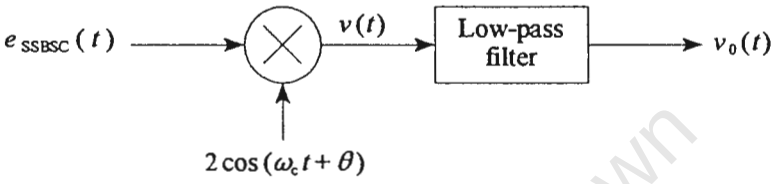

Figure 7.1: Coherent demodulation of a SSBSC signal.

The locally generated carrier has a priori knowledge of the original carrier frequency, but has an arbitrary phase difference θ, measured with respect to the carrier. The SSBSC modulated signal, $e_{SSBSC}(t)$ containing only the upper sideband, can be formally described in canonical form as [25]:

$$s_{USB}(t) = A_c m(t)\cos(\omega_c t) - A_c \hat{m}(t)\sin(\omega_c t) \tag{7.1}$$

Denoting the locally generated carrier as $2\cos(\omega_c t + \theta)$, the output of the multiplier is given by

$$\begin{aligned} v(t) &= s_{USB}(t) \times 2\cos(\omega_c t + \theta) \\ &= [A_c m(t)\cos(\omega_c t) - A_c \hat{m}(t)\sin(\omega_c t)]\,2\cos(\omega_c t + \theta) \\ &= 2A_c m(t)\cos(\omega_c t + \theta)\cos(\omega_c t) - 2\,A_c \hat{m}(t)\cos(\omega_c t + \theta)\sin(\omega_c t) \\ &= A_c m(t)[\cos(\omega_c t + \theta + \omega_c t) + \cos(\omega_c t + \theta - \omega_c t)] \\ &\quad - A_c \hat{m}(t)[\sin(\omega_c t + \theta + \omega_c t) - \sin(\omega_c t + \theta - \omega_c t)] \\ &= A_c m(t)\cos(2\omega_c t + \theta) + A_c m(t)\cos(\theta) \\ &\quad + A_c \hat{m}(t)\sin(\theta) - A_c \hat{m}(t)\sin(2\omega_c t + \theta) \end{aligned} \tag{7.2}$$

The components at twice the carrier frequency are eliminated by the low-pass filter, resulting in the demodulated signal $v_0(t)$ given by

$$v_0(t) = A_c[m(t)\cos(\theta) + \hat{m}(t)\sin(\theta)] \tag{7.3}$$

The demodulated signal $v_0(t)$ of equation (7.3) contains an unwanted component proportional to $\hat{m}(t)\sin(\theta)$, which cannot be removed by the low-pass filter. This unwanted component appears as phase distortion and is caused by the phase error of the locally generated carrier signal.

For a perfectly coherent locally generated carrier, that is, no frequency or phase errors, the demodulated signal is

$$v_0(t) = A_c m(t) \tag{7.4}$$

It is very clear from equation (7.3), that any phase errors in the locally generated carrier will cause phase distortion of the demodulated signal. The larger the phase error the greater the distortion. Transforming equation (7.3) gives [16]:

$$E_0(\omega) = \begin{cases} A_c M(\omega) e^{j\theta} & \omega > 0 \\ A_c M(\omega) e^{-j\theta} & \omega < 0 \end{cases} \tag{7.5}$$

Equation (7.5) shows that $v_0(t)$ has the same magnitude spectrum as that of $m(t)$, but the phase of each component is shifted by θ. For digital modulation systems such as VPSK, it is vital to have minimal phase error in the locally generated carrier for optimum demodulation to be accomplished.

7.2 Deriving the Locally Generated Carrier in the Simulation

7.2.1 Present Method of Carrier Synchronisation in VPSK Systems

Present VPSK digital modulation schemes developed by Walker [4][5], use a PLL in the receiver to lock the locally generated carrier to an integer multiple of the symbol clock signal, which is present in the transmitted signal. This locally generated carrier, which is synchronised to the symbol clock frequency, is used for coherent demodulation of the VPSK modulated signal. This method of synchronisation may break down if the channel is a noisy multi-path environment or has any significant doppler shift [10].

7.2.2 Proposed Method of Carrier Synchronisation

In an effort to overcome the effects of using single sideband suppressed carrier modulation, where there is a total loss of carrier in the transmitted signal, the fundamental purpose of this dissertation is to investigate and find a solution, using direct sequence spread spectrum techniques, to the problem of carrier synchronisation.

The method used in this dissertation is to reference the locally generated carrier to the chip clock signal oscillator in the delay-locked PN code tracking loop. The PN code clock frequency was made a function of the original carrier frequency in the transmitter, which was also a multiple of the symbol clock frequency. Some additional advantages of this approach are as follows:

- the inherent interference rejection properties, for intentional and unintentional interference, of spread spectrum techniques
- multi-path interference rejection
- possibility of secure communications provided by the low probability of intercept characteristics of spread spectrum
- multiple access applications using CDMA (code division multiple access) techniques

This method of carrier synchronisation and demodulation is presented in the following section.

7.3 Demodulation of the VPSK Signal

The locally generated chip clock signal is forced into coherency with the original transmitter by the full-time early-late delay-locked PN code tracking loop discussed in chapter 6. This chip signal is now squared to produce a component at twice the chip clock rate. The output of the squarer, implemented in the simulation by multiplying the chip signal by itself using a multiplier token, is then band pass filtered to provide the locally generated carrier. This process is illustrated in figure 7.2.

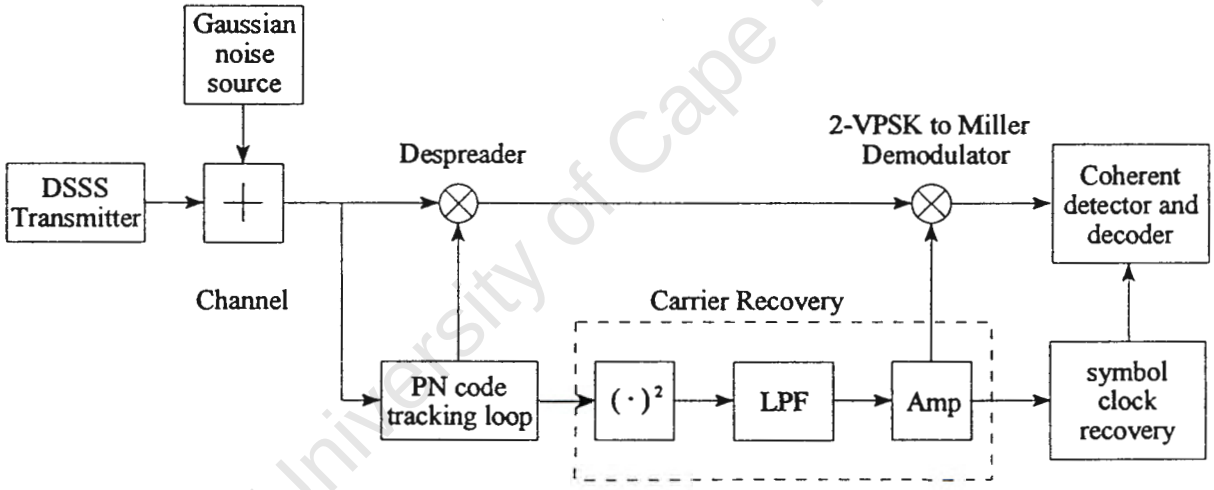

Figure 7.2: Carrier recovery and coherent demodulation in the simulation.

The Band pass filter for selecting the squared chipping frequency component at the output of the multiplier was implemented using a linear phase 8-pole bandpass filter, selected from the analog (continuous) filter library within the linear system token, selected from the generic operator token library. The magnitude and phase plot of this filter is shown in figure 7.3

Figure 7.4 shows an overlay of the original and locally generated carrier signals. It is clear from this figure that perfect synchronisation was accomplished.

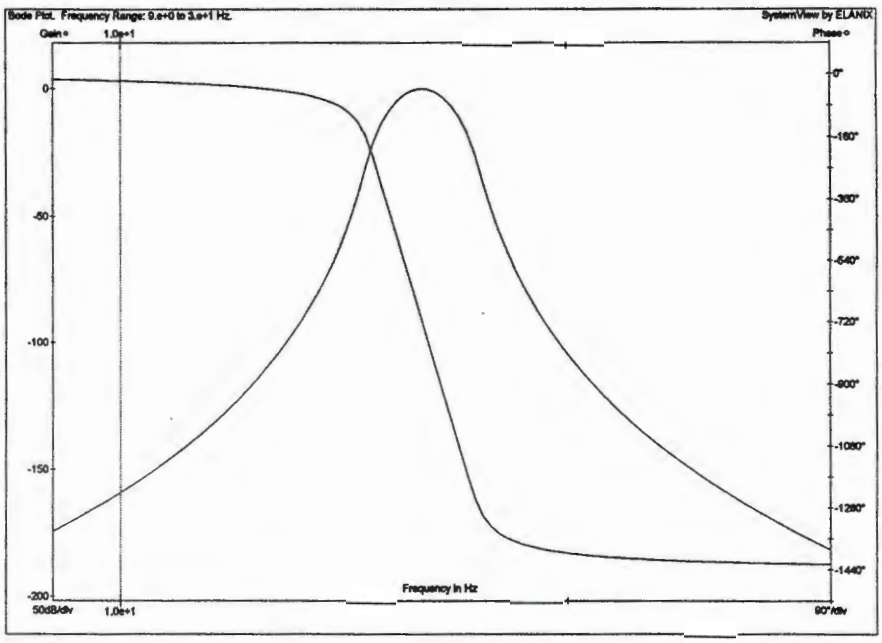

Figure 7.3: Magnitude and phase plot of carrier recovery filter.

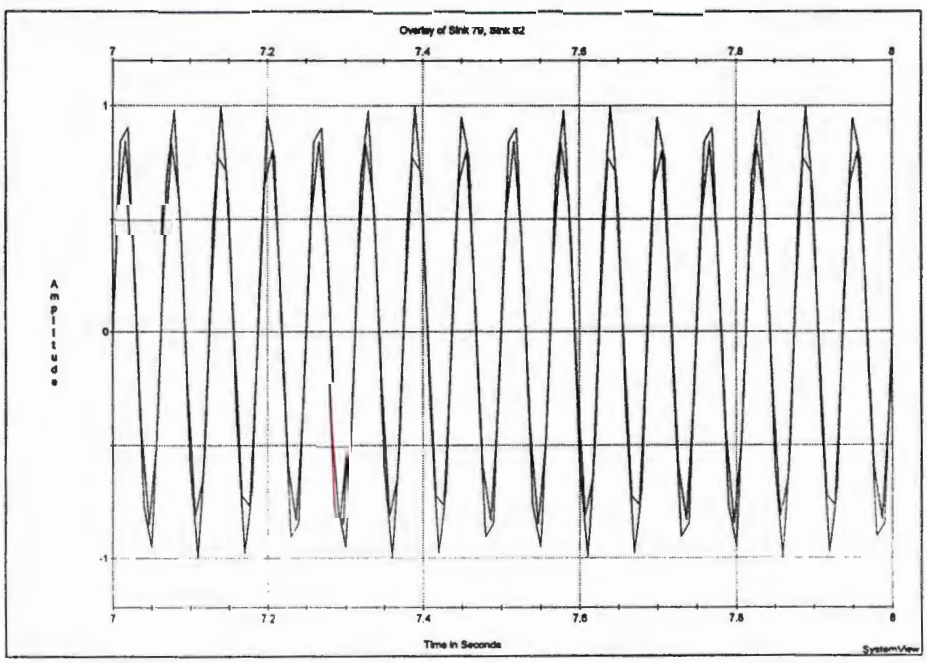

Figure 7.4: Overlay of original and locally generated carrier signals.

The locally generated synchronous carrier was applied to the multiplier, as shown in figure 7.2, for coherent demodulation of the VPSK signal. The down converted baseband information at the output of the multiplier is then selected using a low-pass filter. This low-pass filter was implemented using a Raised Cosine Parametric FIR (finite impulse response) filter to minimise any inter-symbol interference. The design of this Raised Cosine filter was once again performed in the filters and linear systems token selection of SystemView. These Raised Cosine filters are low-pass filters with a cosine-shaped transition band. The FIR filter specifications were selected as:

- Roll-off Factor 0.35
- Nº of FIR taps 129
- Relative BW (R_b/F_s) 0.005
- Input sample rate (F_s) 100 Hz

Figure 7.5 shows the magnitude response of this Raised Cosine FIR filter.

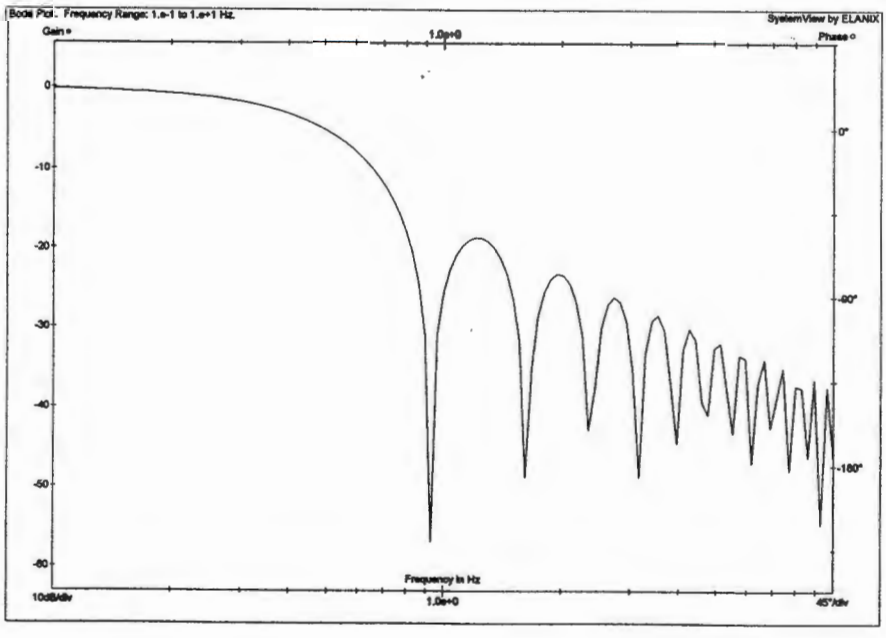

Figure 7.5: Magnitude response of the Raised Cosine FIR filter.

The magnitude spectrum of information translated back down to baseband is shown in figure 7.6. This figure clearly shows that this information is the Miller encoded baseband signal, originally generated in the transmitter. Thus synchronous demodulation of the transmitted VPSK signal has been accomplished.

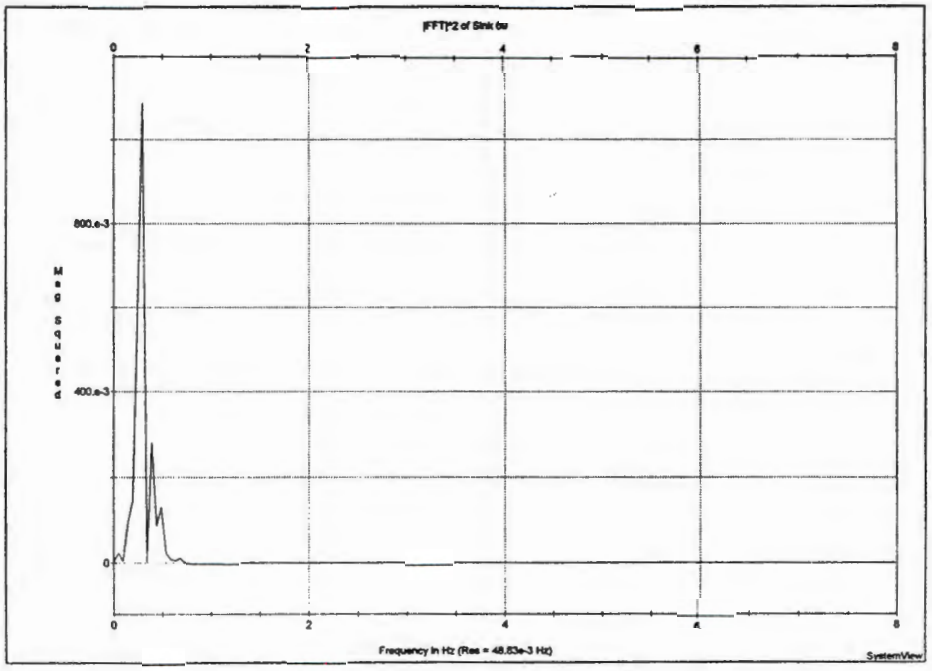

Figure 7.6: Magnitude spectrum of the down-converted Miller code.

Chapter 8

Soft Decision Detection and Decoding of the Miller Line Code

A basic issue in the design of receivers is the detecting of signals corrupted in additive noise. The purpose of detection is to establish the presence or absence of a signal in noise. To enhance the signal to noise ratio and thereby promote the detection process, a detection system usually consists of a pre-detection filter followed by a decision device. When the power spectral density of the noise is constant, that is, the noise is additive white Gaussian noise, the optimum solution for the pre-detection filter is a matched filter [25]. A matched filter is optimum in the sense that it maximises the output signal to noise ratio.

Another approach to optimum detection is based on a probabilistic criterion, directly related to performance ratings of digital communication systems. The probabilistic approach yields the so-called correlation receiver, which involves the correlation of the received signal with a stored replica of the transmitted signal. The matched filter method of optimum detection is equivalent to the correlation approach in the case of additive white Gaussian noise [25].

The demodulation of the 2-VPSK signal incorporated the translation of the Miller line code back down to baseband frequencies. The optimum detection of this AWGN corrupted Miller line code is presented in the following section.

8.1 Detection of Binary Signals in Additive White Gaussian Noise

The detection process consists of two separate steps. The first step consists of reducing the received waveform, $r(t)$ to a single number, $z(t = T_b)$. This operation can be performed by a correlator whose initial conditions are set to zero, just prior to the arrival of each new symbol. At the end of each symbol duration, T_b, the output of the correlator yields the sample $z(T_b)$, sometimes called the test statistic.

The second step of the signal detection process consists of comparing the test statistic, $z(T_b)$, to a threshold level, γ, in order to estimate which signal has been transmitted. Once the received waveform, $r(t)$, is transformed to a number $z(T_b)$, the actual shape of the waveform is no longer important as all waveform types that are transmitted to the same value of $z(T_b)$ are identical for detection purposes. The correlator implementation of the matched filter receiver, maps all signals of equal energy into the same point, $z(T_b)$. This means that it is the signal energy, not the shape of the received waveform that is the important parameter in the detection process [21]. The two step process described above is illustrated in figure 8.1.

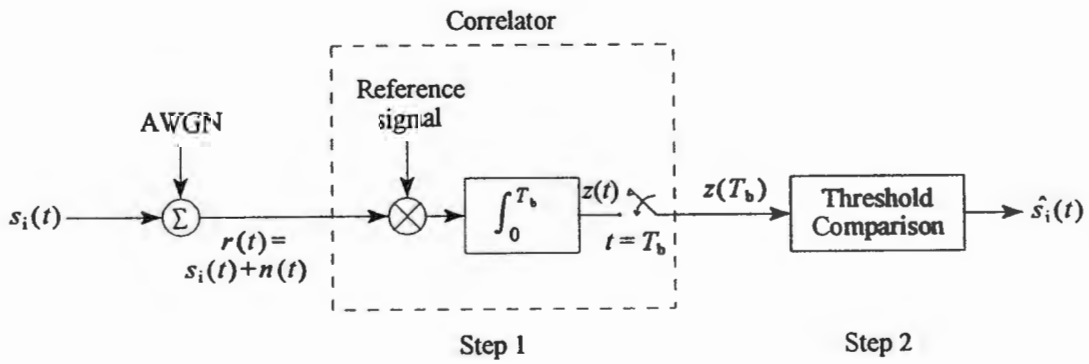

Figure 8.1: Two basic steps in digital signal detection.

This two step process facilitates the decoding of the Miller line code to a bipolar NRZ signal in the detection process, provided the correct reference signals are used.

8.1.1 Correlation Receiver Topology for Detection of a Miller Code

In chapter 2, the Miller line code was described by four types of bit intervals or states, restated here as: (+1, +1); (+1, -1); (-1, +1) and (-1,-1). By choosing the two possible levels as -1 and +1, the four elementary signals which represent a binary 1 and 0 respectively, in a Miller line code, are defined by

$$s_1(t) = -s_4(t) = A \qquad \text{for } 0 \le t \le T_b \tag{8.1}$$

for a binary 0 and

$$s_2(t) = -s_3(t) = \begin{cases} +A & \text{for } 0 \le t < \frac{T_b}{2} \\ -A & \text{for } \frac{T_b}{2} \le t \le T_b \end{cases} \tag{8.2}$$

for a binary 1.

The received signal $r(t)$, which is corrupted by noise is represented by

$$r(t) = s_i(t) + n(t) \qquad i = 1,2,3 \text{ or } 4; \qquad 0 \le t \le T_b \tag{8.3}$$

where

$n(t)$ is a zero mean additive white Gaussian process

$s_i(t)$ is one of the four possible elementary signals in a Miller code

Given the four possible input signals, and referring to figure 8.1, the output of the correlator is given by

$$z_i(t) = \int_0^t r(\tau)\, s_j(\tau)\, d\tau \tag{8.4}$$

where $s_j(t)$ is one of two possible replicas of the transmitted waveform. Thus, the signal $s_i(t)$ whose correlation with the received signal $r(t)$, yields the maximum output $z_i(t)$, is the signal that matches $r(t)$ better that any of the other $s_j(t)$, $j \neq i$

Thus the output of the correlator at $t = T_b$ is

$$z_i(T_b) = a_i(T_b) + n(T_b) \tag{8.5}$$

where $a_i(T_b)$ is the signal component and $n(T_b)$ is the noise component. $z_i(T_b)$ is a sampled number which represents a random process because it was derived from the random process $r(t)$, via a correlator which performs a linear operation. The correlator is a linear time-invariant system [25].

To facilitate the decoding of the Miller signal in the detection process, the correlator output $z_i(T_b)$, must be assigned to one of the two elementary signals that represent a bipolar NRZ signal. The following assignments were made for the conversion from Miller code to NRZ code:

$$\begin{aligned} &[s_1(t); s_4(t)] \quad \text{assign } -A \qquad 0 \le t < T_b \\ &[s_2(t); s_3(t)] \quad \text{assign } +A \qquad 0 \le t \le T_b \end{aligned} \tag{8.6}$$

The above assignments imply that the detector must provide, at its output, an antipodal set of estimates, given by $\hat{s}_1(t) = +A$ and $\hat{s}_2(t) = -A$ for $0 \le t \le T_b$, to achieve the required decoding. The reference signals required to implement the decoding are given by

$$\bar{s}_1(t) = \begin{cases} +A & \text{for} \quad 0 \le t < \frac{T_b}{2} \\ -A & \text{for} \quad \frac{T_b}{2} \le t \le T_b \end{cases} \tag{8.7}$$

for a binary 1, and

$$\bar{s}_2(t) = +A \qquad \text{for } 0 \le t \le T_b \tag{8.8}$$

for a binary 0.

These reference signals are a priori information in the receiver and $\bar{s}_1(t)$ can be implemented using the recovered clock signal

Figure 8.2 shows the block diagram of a combined correlation receiver and decoder for detection and decoding of a Miller line code.

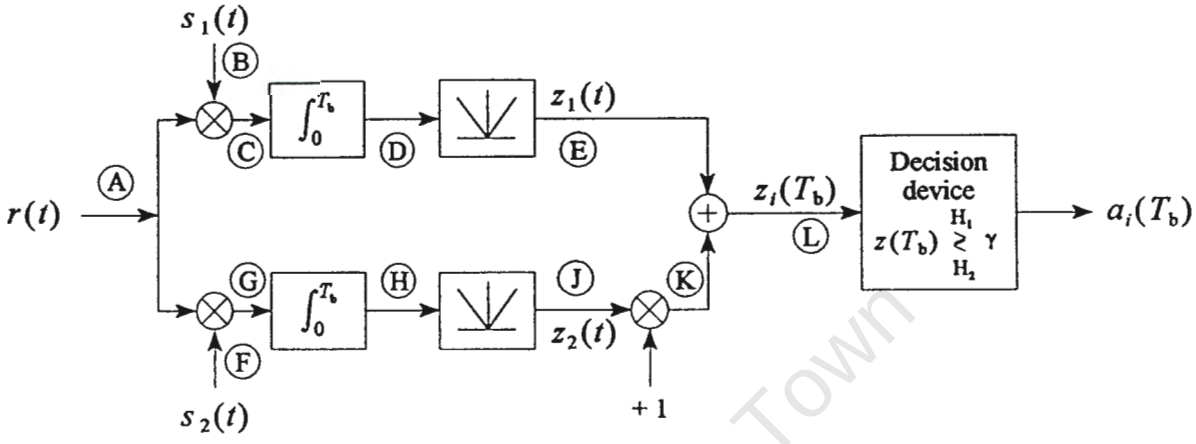

Figure 8.2: Optimum detector and decoder for Miller to NRZ code.

The operation of this optimum detector is illustrated in figure 8.3, where the waveforms at the input and output of each block, for a received Miller code sequence, are presented. For simplicity, the signal level chosen, and used in the simulation, has an amplitude of $\pm$ 1 volt. This detector/decoder will also perform optimally if the reference signals were the converse of those presented, since the absolute values of the signals at the output of the correlators and the sampled integrators are used.

It is absolutely clear from figure 8.3 that this detector/decoder is optimum, because it utilises the total energy in the received Miller code to maximise the signal to noise ratio at the input to the decision device. The final waveform is an antipodal NRZ data signal which is presented to the decision device.

Each waveform is referenced to the input and output of each block in figure 8.2 alphabetically to facilitate easy cross-referencing.

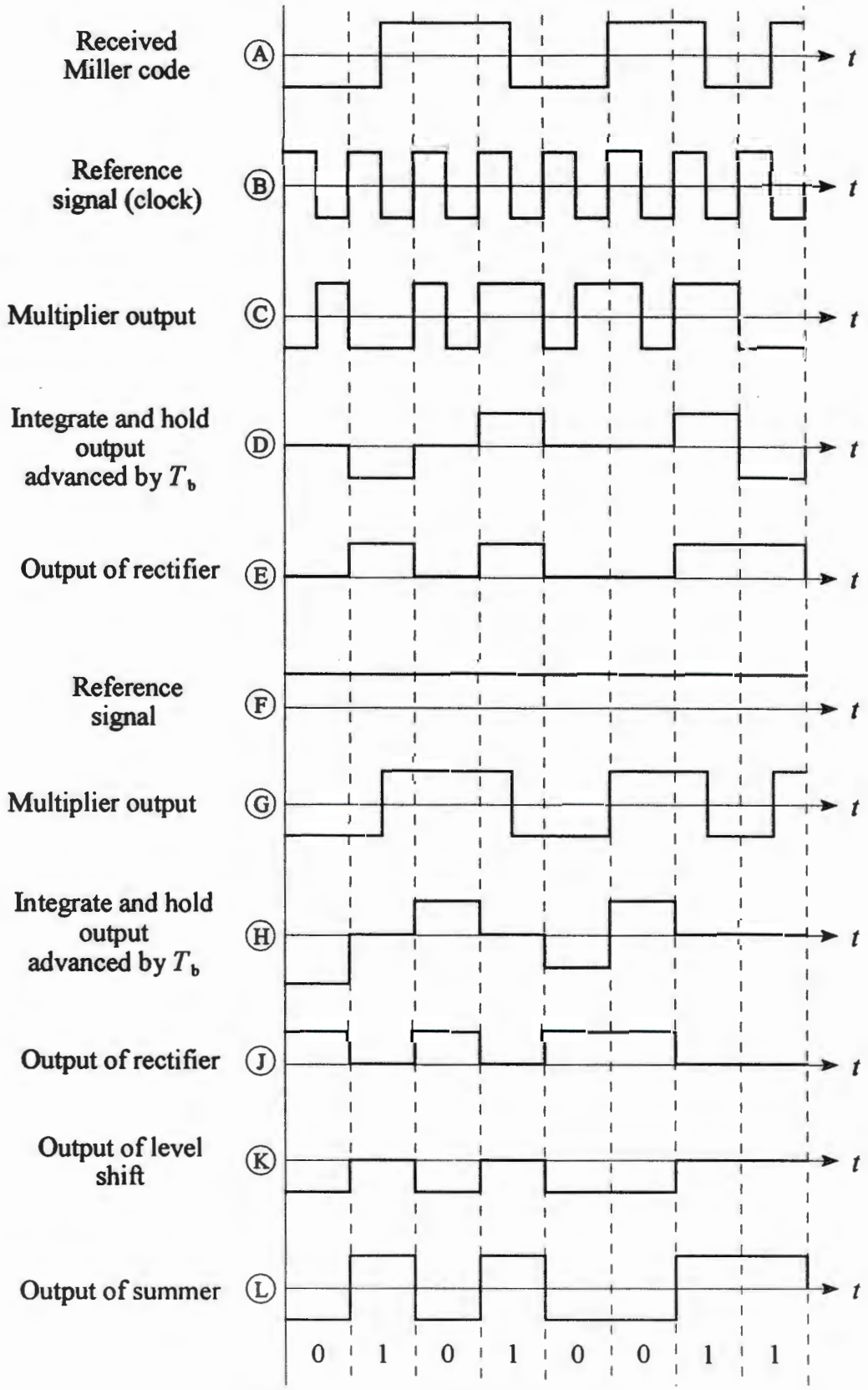

Figure 8.3: Waveforms within the optimum Miller detector and decoder.

8.1.2 Maximum Likelihood Structure for the Decision Device

The second step of the signal detection process consists of comparing the test statistic, $z(T_b)$, to a threshold level, γ in the decision device, in order to estimate which signal, $s_1(t)$ or $s_2(t)$ has been transmitted. The filtering process of the first step is independent of the decision criterion of the second step in the detection process and thus also independent of the choice of the threshold setting, γ. The final step in the detection process is to make the decision

$$z(T_b) \underset{H_2}{\overset{H_1}{\gtrless}} \gamma \tag{8.9}$$

where H_1 and H_2 are the two possible binary hypotheses. Choosing H_1 is equivalent to deciding that signal $s_1(t)$ was sent, and choosing H_2 is equivalent to deciding that signal $s_2(t)$ was sent. The inequality relationship indicates that hypothesis H_1 is chosen if $z(T_b) > \gamma$, and hypothesis H_2 is chosen if $z(T_b) < \gamma$. If $z(T_b) = \gamma$, the decision is arbitrary.

Referring to figure 8.1, the output of the of the correlator , sampled at $t = T_b$ yields

$$z_i(T_b) = a_i(T_b) + n(T_b) \qquad i = 1,2 \tag{8.10}$$

The noise component is a zero-mean Gaussian random variable and thus $z_i(T_b)$ is a Gaussian random variable with a mean of either a_1 or a_2, depending on whether a binary one or zero was sent. The conditional probability density functions, $p(z|s_1)$ and $p(z|s_2)$ are given by [21]

$$\begin{aligned} p(z|s_1) &= \frac{1}{\sigma_0\sqrt{2\pi}} \exp\left[-\frac{1}{2}\left(\frac{z-a_1}{\sigma_0}\right)^2\right] \\ p(z|s_2) &= \frac{1}{\sigma_0\sqrt{2\pi}} \exp\left[-\frac{1}{2}\left(\frac{z-a_2}{\sigma_0}\right)^2\right] \end{aligned} \tag{8.11}$$

and are illustrated in figure 8.4.

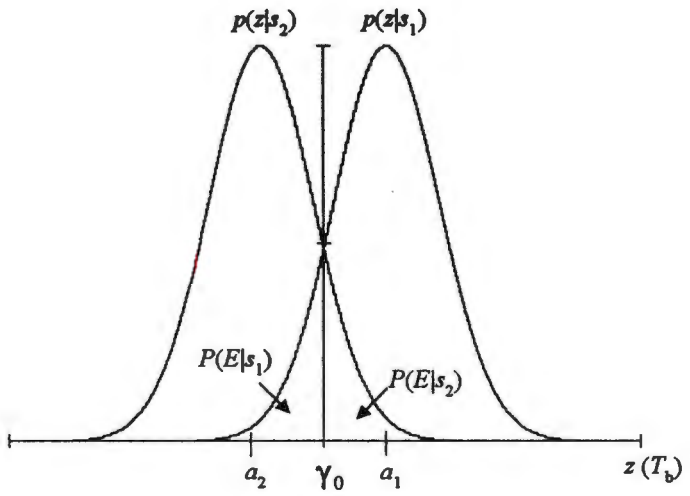

Figure 8.4: Conditional probability density function: $p(z|s_1)$ and $p(z|s_2)$.

Figure 8.4 shows two ways that an error can be made:

- if $s_1(t)$ was sent and $z_1(T_b) = a_1(T_b) < \gamma_0$, or
- if $s_2(t)$ was sent and $z_2(T_b) = a_2(T_b) > \gamma_0$.

The corresponding probabilities of error are shown in figure 8.4 and are given by [21][26]

$$P(E|s_1) = \int_{-\infty}^{\gamma_0} p(z|s_1)\,dz \tag{8.12}$$

for $s_1(t)$ present, and

$$P(E|s_2) = \int_{\gamma_0}^{\infty} p(z|s_2)\,dz \tag{8.13}$$

for $s_2(t)$ present.

If the a priori probabilities that $s_1(t)$ and $s_2(t)$ were sent are equally likely, then the optimum

choice for the threshold in terms of minimising the probability of error P_E is [26]

$$\gamma_0 \text{ (opt)} = \frac{a_1 + a_2}{2} \tag{8.14}$$

In this case, the received waveform is a bipolar format, which implies that $a_1 = -a_2$, and therefore the optimum decision threshold is $\gamma_0 = 0$. Thus the total probability of error is given by Bayes theorem as [21][26]

$$P_E = P(E|s_1)P(s_1) + P(E|s_2)P(s_2) \tag{8.15}$$

Since in this case, the a priori probabilities $P(s_1)$ and $P(s_1)$ are equal, that is, the data stream consists of equally likely bits, and thus $P(s_1) = P(s_1) = ½$. Moreover, the probability density functions are symmetrical around γ_0 resulting in the total probability simplifying to

$$P_E = P(E|s_1) = P(E|s_2) \tag{8.16}$$

which implies that P_E is given by equations (8.12) and (8.13). Replacing the likelihood probability density functions, $p(z|s_1)$ and $p(z|s_2)$ by their Gaussian equivalents given in equation (8.11), the P_E is given by [21][26]

$$P_E = Q\left[\frac{a_1 - a_2}{2\sigma_0}\right] \tag{8.17}$$

where $Q(x)$, called the complimentary error function, describes the area beneath the tail of the Gaussian probability density distribution functions, and is defined by [21]

$$Q(x) = \frac{1}{\sqrt{2\pi}} \int_x^\infty \exp\left[-\frac{u^2}{2}\right] du \tag{8.18}$$

$Q(x)$ cannot be evaluated in closed form, and is presented in tabular form or determined using

good approximations of $Q(x)$ by simpler functions [21].

The argument of $Q(x)$ in equation (8.17) can be expressed, in terms of the instantaneous signal power and average noise power at $t = T_b$ at the output of the detector, as [21]

$$\left(\frac{S}{N}\right)_{T_b} = \frac{2E_b}{N_0} \tag{8.19}$$

giving

$$P_E = Q\left[\sqrt{\frac{2E_b}{N_0}}\right] \tag{8.20}$$

where $E_b = A^2 T_b$ is the average energy per bit at the input to the detector, and $N_0/2$ is the two sided power spectral density of the noise at the input to the detector.

8.2 Symbol Clock Synchronisation for a Miller Line Code

In order to be able to generate the reference signals necessary for the demodulation, the phases of which must be identical to the phases of the signalling alphabet used in the transmitter, the receiver has to be in synchronisation with the received carrier. This means that there has to be phase concurrence between the received carrier signal and the replica of it in the receiver. This matter was addressed in chapters 6 and 7 of this dissertation.

Once the received signal has been demodulated back down to baseband, it is necessary to recover the symbol clock signal. This symbol clock signal is required to determine the integration limits and hence the sampling points in the detection process. Also, for the Miller encoded signal, the symbol clock is needed as one of the reference signals.

In existing VPSK modulation schemes, the inventor states that the spectrum generated by the

VPSK signal has a large spectral component at twice the data rate [8]. He uses this component to achieve symbol clock synchronisation in the receiver. However, in this dissertation, since the original carrier and PN chipping frequency were made functions of the symbol clock frequency in the transmitter, symbol clock recovery and carrier recovery in the receiver are derived from the PN code tracking loop used for the despreading of the received spread carrier. This method of symbol clock recovery is presented in the following section.

8.2.1 Symbol Clock Recovery in the Simulation

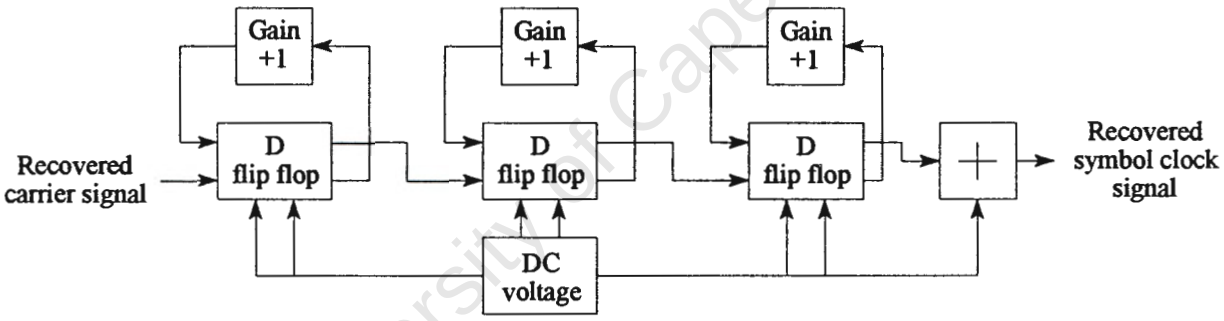

Figure 8.5: Symbol clock recovery in the simulation.

In chapter 7 the method used to derive the locally generated carrier was described. This process involved the use of an early-late non-coherent delay-locked tracking loop. In the relevant literature, Sklar [21] explains the use of both open-loop and closed-loop symbol synchronisers. Interestingly, the implementation of a closed loop symbol synchroniser described in Sklar [21] is an early-late gate data synchroniser. Thus, the method of symbol clock recovery used in this dissertation is a closed loop symbol synchroniser, but implemented at a slightly higher frequency than the original symbol clock frequency.

The synchronised replica of the received carrier derived from the PN code tracking loop and discussed in chapter 7, is now used to recover the symbol clock signal. This locally generated carrier of 8 Hz in the simulation, is divided down by eight to give the symbol clock of 1 Hz. This division was implemented using three D-flip-flops, each connected as a divide by two and selected from the logic library within SystemView, as shown in figure 8.5. The output of the last D-flip-flop is level shifted to give a bipolar symbol clock signal at 1 Hz. The recovered symbol clock signal is shown in figure 8.6.

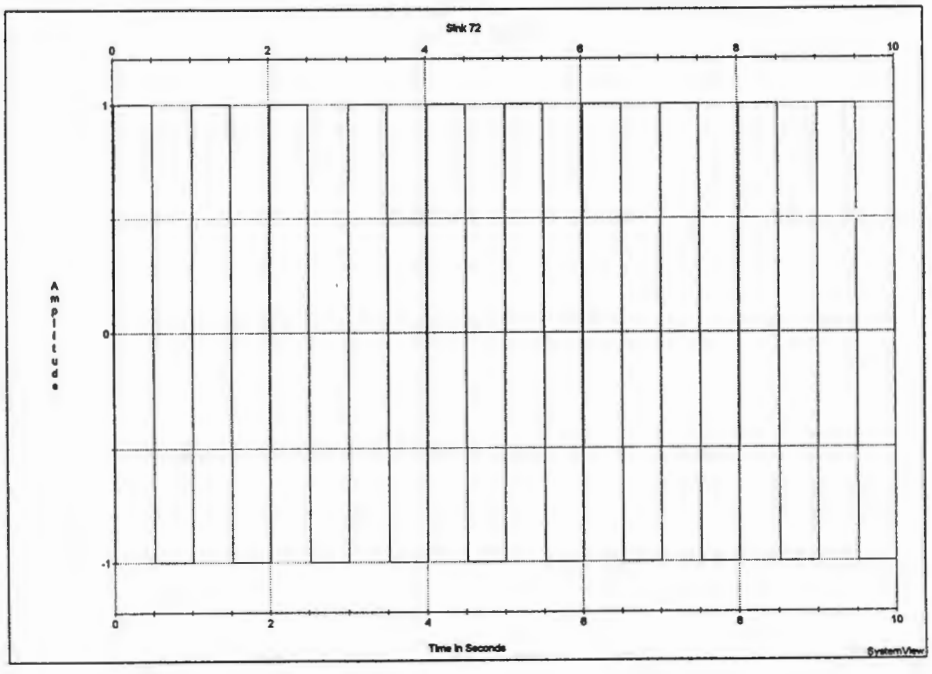

Figure 8.6: Recovered symbol clock signal.

8.3 Detection and decoding as Implemented in the Simulation

The block diagram of the Miller to NRZ detector and decoder is shown in figure 8.7. The correlation receiver section was implemented as shown in figure 8.2, except the reference signal $\bar{s}_2(t)$ was not implemented. The reason therefore is readily seen by comparing waveform A and waveform G of figure 8.3. The signal in waveform G is exactly the same signal as the incoming Miller line encoded signal and thus the reference and the relevant

multiplier are not required.

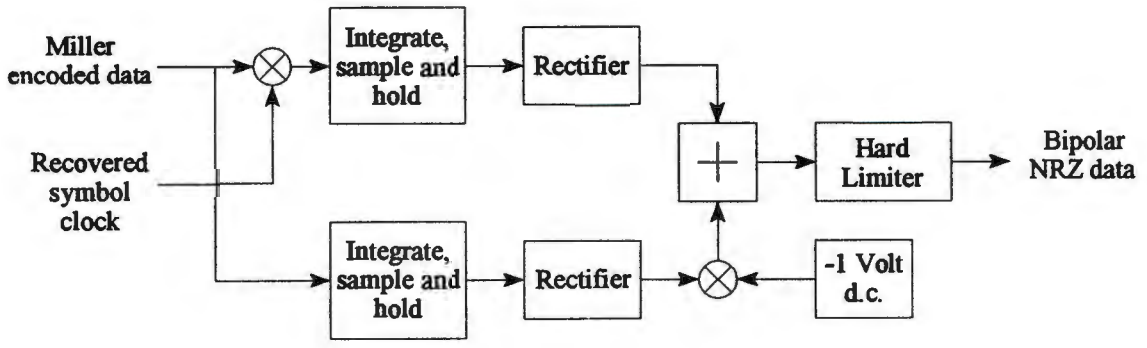

Figure 8.7: Block diagram of the detector and decoder implemented in the simulation.

The multiplier token was selected from the generic library of tokens. The integrator tokens were selected from the communication library as integrate and dump functions with the following parameters:

- integration time = 1 sec, which is the bit period in this simulation
- offset = 0 sec
- output = hold value. The output of the filter is held until the next sample.

The magnitude of the output signals of the integrators were implemented by selecting a rectifier token from the function library. The level shifter in the bottom loop was implemented by applying the integrator output to a negative unity gain amplifier selected from the operator library of tokens. The two loops were then added using an adder token from the generic token library. Finally, the decision device was implemented with a hard limiter function token. The input maximum was set to 0 volts, that is the decision threshold, and the output maximum set to ± 1 volt. The output of the limiter is restricted to $\pm$ the output maximum when the input exceeds the input maximum. The recovered bipolar NRZ data signal is shown in figure 8.8 and a cross correlation of the recovered and the original data signal is shown in figure 8.9.

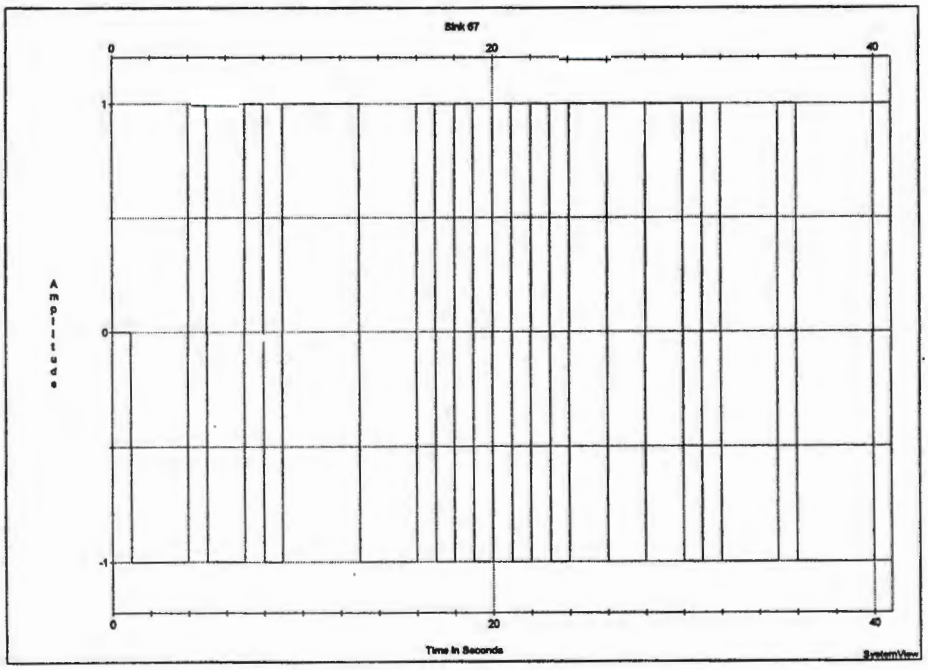

Figure 8.8: Recovered NRZ data signal at output of detector/decoder.

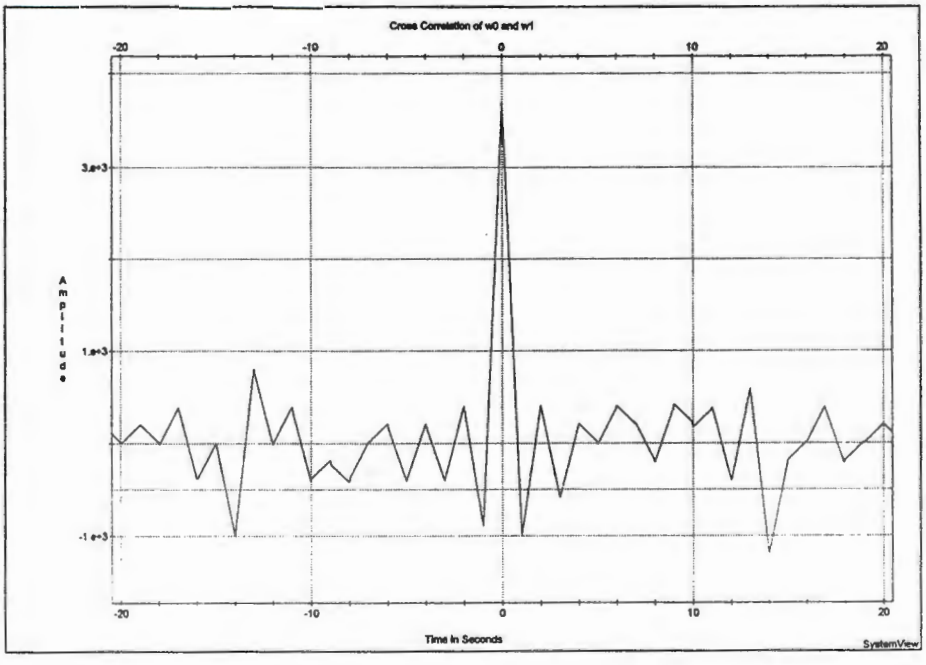

Figure 8.9: Cross-correlation of the original and the recovered NRZ data signals.

8.4 Performance Measurement in the Simulation

The system error performance was determined at four theoretical values of error probability. The results are tabled in table 8.1 and shown graphically in figure 8.10.

Theoretical P_E	E_b/N_0 (dB)	N_0 (W/Hz)	Simulated P_E
1×10^{-3}	6.788	0.20951	0.002
1×10^{-4}	8.3976	0.1446	0.0001
1×10^{-5}	9.5875	0.11	0.0000158
1×10^{-6}	10.53	0.08852	0.000002

Table 8.1: System error performance.

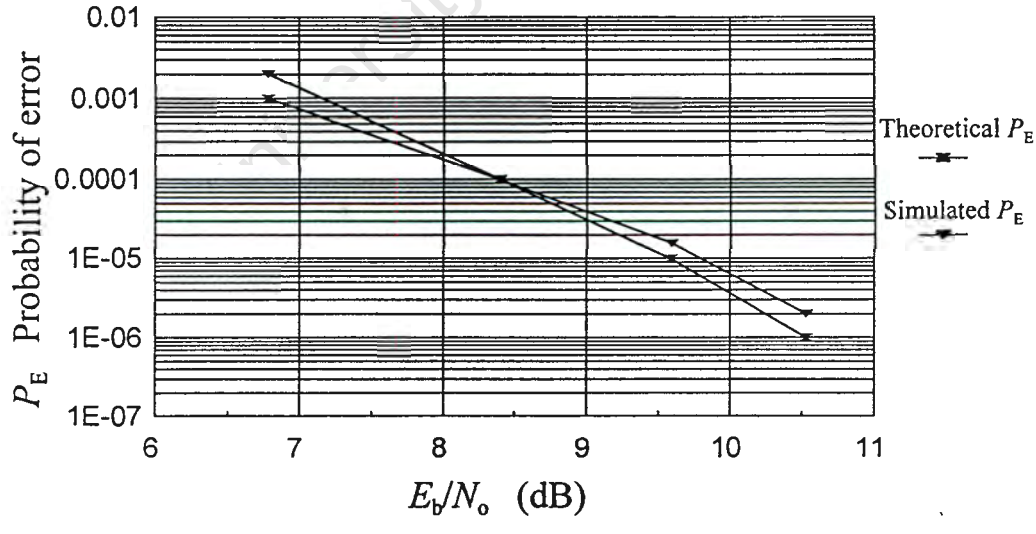

Figure 8.10: Theoretical and simulated error performance.

Chapter 9

Conclusion

In this dissertation, the development of an alternative synchronisation method, using Direct Sequence Spread Spectrum Techniques (DSSS), for the coherent demodulation of a Variable Phase Shift Keyed (2-VPSK) digital modulation signal, was presented.

The major characteristics of the DSSS 2-VPSK system are:

- The system is a coherent system in that the demodulation, detection and decoding are all performed with synchronous locally generated signals.
- The system offers an alternative method of acquiring the synchronous signals required for coherent demodulation in the receiver.
- The early-late delay-locked PN code tracking loop renders an exact replica of the transmitted PN spreading code sequence.
- The spreading and despreading operation on the 2-VPSK signal is transparent to the receiver function in an additive white Gaussian noise environment.
- The locally generated replica of the clock signal used for PN code generation in the transmitter is used to derive the locally generated carrier and symbol clock signals in the receiver.
- The phase-locked loop, in the form of an early-late delay-locked loop, forms the primary control circuit to track variations in phase of an incoming signal.
- The system operated successfully in the presence of AWGN.

To achieve the main purpose of this dissertation, the system in its entirety was designed and then simulated in the SystemView simulation environment. This dynamic system design and analysis tool has the following powerful characteristics:

- The system window within SystemView provides an extremely powerful platform for the conception, design and testing of complex systems.
- The analysis window enables the viewing and analysis of waveforms anywhere within the designed system.
- The sink calculator within the analysis window, provides a very powerful tool for generating frequency spectrums, correlation functions and overlaying of waveforms.
- Many complicated operations, linear and non-linear functions, analog and digital signal processing applications are very easily implemented using a scheme of tokens and libraries.

9.1 Recommendations

This section suggests additional areas of research to further test and analyse the performance of the system.

9.1.1 Detection and Synchronisation of the PN Sequence

In the receiver, it was assumed the PN code sequence acquisition had been performed, that is, the PN code sequence was within one chip period of the locally generated PN code sequence, and only the PN code tracking function was designed and implemented in the simulation. To implement this system in practice, it would be necessary to realize the full acquisition and tracking function in the receiver. Thus, investigations into PN code acquisition would further advance the achievements obtained in this dissertation.

9.1.2 Noise

Although the system functioned in the presence of additive white Gaussian noise, the main attributes of spread spectrum, that is, its inherent interference rejection capabilities , especially the cases of intentional narrow and wide-band interference, have not been ascertained. Investigations into the performance of the system to determine its capabilities in the presence of these types of interference, as well as the effects of multi-path channel characteristics also needs further investigation.

9.1.3 System Complexity and Improvements

Variable Phase Shift Keying is a relatively unknown digital modulation scheme with excellent spectral characteristics. The DSSS 2-VPSK system designed in this thesis is only a basic system and could turn out to be a rather complex, yet very attractive digital communications system. The additional complexity of spread spectrum techniques is to a large extent neutralised by the possible improvement in system performance in non-Gaussian type environments. With more investigation into these areas it is believed that this digital modulation scheme can be implemented in CDMA (code-division multiple access) applications.

Appendix A

2-VPSK DSSS System Block Diagram

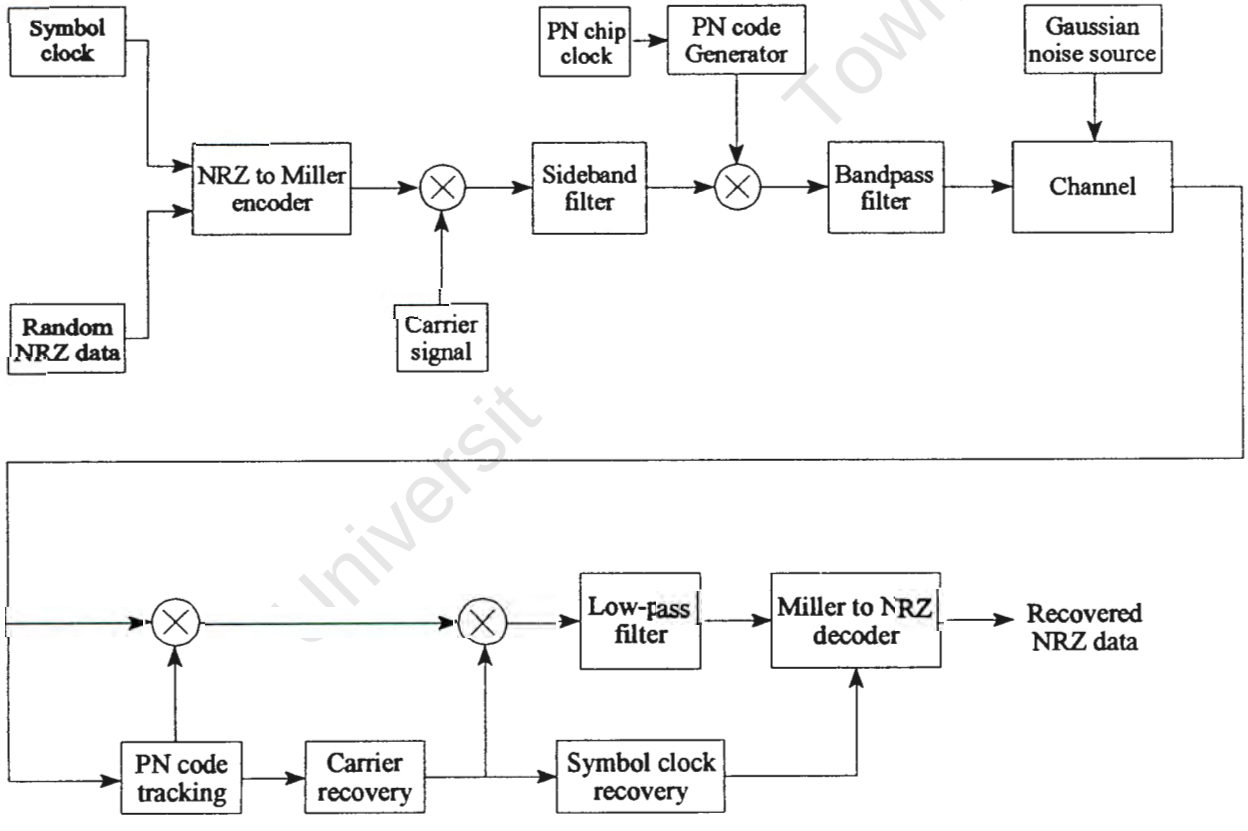

Appendix B

SystemView Simulation Package

SystemView by Elanix is a dynamic systems analysis tool for the design and simulation of engineering systems. SystemView provides a sophisticated analysis engine, embedded in the user-friendly and powerful Windows environment, for simulation of analog filter design, DSP filters, control systems and communication systems. Complex systems can be designed and tested using a system of tokens and MetaSystems. After simulation, an analysis window is generated where system waveforms can be examined.

Tokens are the building blocks of all SystemView simulations. The available token reservoir contains eight generic tokens representing eight different token classes:

- Source token: represents a library of sources used to generate system inputs.
- MetaSystem: represents a group of tokens which make up a complete subsystem,function or process in a simulation.
- Adder token: forms the sum of its inputs.
- Operator token: represents a library of operators which use input data as the argument for the operation.
- Function token: represents a library of functions which use input data as the argument for the operation.
- Multiplier token: forms the products of its inputs.
- Sink token: represents a library of Sinks for collecting, displaying, analysing the signals within a system.

The available token libraries, which contain comprehensive sets of tools to aid the design of systems, are:

- The logic library
- The Communications library
- The RF/analog library
- The DSP library

SystemView is inherently a discrete time system simulator. System time is controlled by clicking on the system time button and allows the control of:

- Start and stop time.
- Sample rate and time spacing
- Number of samples
- Frequency resolution

The analysis window is the primary tool for viewing and processing Sink data, and provides a very flexible method to examine system waveforms.

References

[1] A. Miller. *Recording and or Reproducing System.* United States Patent, October 1963. Patent Number 3,108,261.

[2] H.R. Walker. *The Advantages of VPSK Modulation for Data Transmission.* Pegasus Data Systems, 562 Lincoln Boulevard, Middlesex, New Jersey 08846.

[3] H.R. Walker. *VPSK Modulation, A Tutorial.* Pegasus Data Systems, 562 Lincoln Boulevard, Middlesex, New Jersey 08846.

[4] H.R. Walker. *High Speed Binary Data Communication System.* United States Patent, May 1988. Patent Number 4,742,532.

[5] H.R. Walker. *High Speed Data Communication System using Phase Shift Key Coding.* United States Patent, February 1993. Patent Number 5,185,765.

[6] J.D. Gibson. *The Mobile Communications Handbook.* CRC Press Inc., 1996.

[7] R.C. Dixon. *Spread Spectrum Systems.* John Wiley and Sons, 1976.

[8] B. Stryzak and H.R. Walker. *Improve Data Transmissions Using Single-Sideband FM with Suppressed Carrier.* Microwave and RF Magazine, November 1994.

[9] J.G. van de Groenendaal. *Novel Low Cost Synchronisation Network for Spread Spectrum Systems.* Doctoral Thesis, University of Cape Town, 1995.

[10] R.M. Braun. *Report on VPSK for Plessey-Telumat.* Technical Report, Digital modulation Research Group, University of Cape Town, March 1996.

[11] N.Q. Duc and B.M. Smith. *Line Coding for Digital Data Transmission.* A.T.R. Volume 11, Number 2, Telecom Australia Research Laboratories, 1977.

[12] F.G. Stremler. *Introduction to Communication Systems.* Third Edition. Addison-Wesley, 1989.

[13] M. Hecht and A Guida. Delay Modulation. *Proceedings of the IEEE*, Proceedings Letters, Volume 57, pages 1314-1316, July 1969.

[14] R.C. Titsworth and L.R. Welch. *Power Spectra of Signals Modulated by Random or Pseudo-random Sequences*. Technical Report Number 32-140, Jet Propulsion Laboratory, Pasadena, California, October 1961.

[15] W.C. Lindsay and M.K. Simon. *Telecommunication Systems Engineering*. Prentice Hall Inc., Englewood Cliffs, New Jersey, 1973.

[16] B.P. Lathi. *Modern Digital and Analog Communication Systems*. Second Edition. Saunders College Publishing, 1989.

[17] M.S. Roden. *Analog and Digital Communication Systems*. Third Edition. Prentice Hall Inc., Englewood Cliffs, New Jersey, 1991.

[18] L. W. Couch II. *Modern Communication Systems, Principles and Applications*. Prentice Hall Inc., Englewood Cliffs, New Jersey, 1995.

[19] R.L. Peterson, R.E. Zeimer and D.E. Borth. *Introduction to Spread Spectrum Communications*. Prentice Hall Inc., Englewood Cliffs, New Jersey, 1995.

[20] R.L Peterson and R.E. Zeimer. *Digital Communications and Spread Spectrum Systems*. Macmillan Publishing Company, New York, 1985.

[21] B. Sklar. *Digital Communications, Fundamentals and Applications*. Prentice Hall Inc., Englewood Cliffs, New Jersey, 1988.

[22] T.S. Rappaport. *Wireless Communications, Principles and Practice*. Prentice Hall Inc., Upper Saddle River, New Jersey, 1996.

[23] K. Feher. *Wireless Digital Communications, Modulation and Spread Spectrum Applications*. Prentice Hall Inc., Upper Saddle River, New Jersey, 1995

[24] S.Haykin. *Communication Systems*. Third Edition. John Wiley and Sons, Inc., New York, 1994.

[25] S.Haykin. *An Introduction to Analog and Digital Communications*. John Wiley and Sons, Inc., New York, 1989.

[26] R.E. Zeimer and R.L. Peterson. *Introduction to Digital Communication*. Macmillan Publishing Company, New York, 1992.